# Performance Analysis of Holographic MIMO Based Integrated Sensing and Communications

Boqun Zhao, *Graduate Student Member, IEEE*, Chongjun Ouyang, *Member, IEEE*, Xingqi Zhang, *Member, IEEE*, and Yuanwei Liu, *Fellow, IEEE* 

Abstract—Given the high spectral efficiency, holographic multiple-input multiple-output (MIMO) technology holds promise for enhancing both sensing and communication capabilities. However, accurately characterizing its performance poses a challenge due to the spatial correlation induced by densely spaced antennas. In this paper, a holographic MIMO (HMIMO) based integrated sensing and communications (ISAC) framework is proposed for both downlink and uplink scenarios. The spacial correlation is incorporated in the communication channel modeling, while an accurate spherical wave-based model is utilized to characterize sensing link. By considering both instantaneous channel state information (CSI) and statistical CSI, closed-form expressions are derived for sensing rates (SRs), communication rates (CRs), and outage probabilities under different ISAC designs to investigate the theoretical performance limits of the proposed HISAC framework. Further insights are gained by examining high signal-to-noise ratio slopes and diversity orders. Specifically, i) for the downlink case, a sensing-centric (S-C) design and a communications-centric (C-C) design are investigated based on different beamforming strategies, and a Pareto optimal design is proposed to characterize the attainable SR-CR region; ii) for the uplink case, the S-C design and the C-C design are distinguished by the interference cancellation order of the communication signal and the sensing signal, and the rate region is obtained through a time-sharing strategy. Numerical results reveal that HMIMO based ISAC (HISAC) systems outperform both conventional MIMO based ISAC systems and HMIMO based frequency-division sensing and communications systems, underscoring the superior performance of HISAC.

Index Terms—Holographic multiple-input multiple-output (HMIMO), integrated sensing and communications (ISAC), performance analysis.

#### I. INTRODUCTION

The concept of Integrated Sensing and Communications (ISAC) has attracted substantial attention from both academia and industry, due to its potential contributions to the development of sixth-generation (6G) and future wireless networks [1]. A distinctive feature that sets ISAC apart is its ability to share the same hardware, power, frequency, and time resources for both communication and sensing purposes. This stands in contrast to the conventional approach of Frequency-Division Sensing and Communications (FDSAC), which necessitates isolated infrastructures and frequency ranges for the two functions. Consequently, compared to FDSAC, ISAC is anticipated

B. Zhao and X. Zhang are with Department of Electrical and Computer Engineering, University of Alberta, Edmonton AB, T6G 2R3, Canada (email: {boqun1, xingqi.zhang}@ualberta.ca).

C. Ouyang is with the School of Electrical and Electronic Engineering, University College Dublin, Dublin, D04 V1W8, Ireland, and also with the School of Electronic Engineering and Computer Science, Queen Mary University of London, London, E1 4NS, U.K. (e-mail: chongjun.ouyang@ucd.ie).

Y. Liu is with the School of Electronic Engineering and Computer Science, Queen Mary University of London, London, E1 4NS, U.K. (email: yuanwei.liu@qmul.ac.uk).

to be more effective in terms of spectrum utilization, energy consumption, and hardware requirements [2], [3].

Recently, the emergence of the concept of holographic multiple-input multiple-output (MIMO), inspired by the promising beamforming gains of massive MIMO with its large-scale aperture array, has gained prominence. Holographic MIMO (HMIMO) is characterized by a larger and denser array, containing a substantial quantity of antennas spaced at intervals smaller than half of the wavelength [4]–[6]. This technology has been proposed to significantly enhance the capabilities of wireless transmissions, especially considering its potential integration into 6G networks [4]. Leveraging this advantage, recent work, such as [7], [8], has applied H-MIMO to ISAC, which has demonstrated the potential to enhance the performance of sensing and communications (S&C) through a well-designed beamforming strategy.

However, so far, research on HISAC has been quite limited. The authors of [7] provided comprehensive overviews of hardware structure and working principles for HISAC, identifying challenges and outlining future research opportunities for implementing holographic ISAC networks. A holographic beamforming scheme was proposed for HISAC in [8], proven to outperform the conventional MIMO where thes pacing between antennas is greater than or equal to half a wavelength. The authors of [9] designed an analog and digital beamforming optimization algorithm for a multi-band HISAC system to avoid the physical limitations of ultra-wide bandwidth. While these studies primarily focus on hardware design and beamforming strategies for HISAC, the fundamental performance limits of HISAC is still remain unexplored.

From an information-theoretic perspective, the performance limits of S&C can be evaluated by the sensing rate (SR) and communication rate (CR), respectively [2], [10]. SR measures the system's capability to estimate environmental information via sensing processes, while CR measures the system's capacity for data transmission through communication processes [10]. A comprehensive analysis of these two metrics provides valuable insights into the overall performance and effectiveness of ISAC in seamlessly integrating S&C functions.

Some performance analysis has been conducted for single-antenna and conventional MIMO based ISAC systems. The authors of [11], analyzed performance of ISAC supported by a single-antenna micro base station (BS) under nonorthogonal downlink transmission. In another study, [12], achievable bounds on performance for a receiver that observes communications and radar echo in a same frequency allocation was derived. [13] and [14], considering distinct dual-functional S&C (DFSAC) scenarios, characterized the S&C performance for downlink and uplink cases, respectively, of conventional

MIMO based ISAC, where the communication channels are assumed to be independent and identically distributed (i.i.d.).

However, the distinctive feature of HMIMO lies in the deployment of an exceptionally large number of sub-wavelength spaced antennas, inducing spatial correlation among the antenna elements across the entire array. Consequently, the channel fading within HMIMO exhibits inherent spatial correlation, discouraging the use of the simplistic i.i.d. fading. Owing to this unique characteristic associated with HMIMO, analyzing the S&C performance of proves to be a challenging task and has not been studied yet.

Motivated by the aforementioned research gaps, this article undertakes a comprehensive performance analysis of a HISAC system from the information-theoretic perspective. In an effort to address the challenges arising from the utilization of HMIMO, this article endeavors to derive closed-form expressions for SR and CR, thereby offering insights into the S&C performance of HISAC. The main contributions of this article can be summarized as follows:

- We propose a HISAC framework for both downlink and uplink scenarios, where we accounts for the spatial correlation within the communication channel by leveraging a channel model based on the approximated Fourier planewave series expansion [15]. Meanwhile, we utilize a spherical wave-based free-space deterministic model to describe the sensing link.
- By considering different types of channel state information (CSI) available to the BS, namely instantaneous CSI (I-CSI) and statistical CSI (S-CSI), we derive closed-form expressions for SRs, CRs, and outage probabilities (OPs) based on the proposed channel models and various ISAC designs. For the downlink scenario, we investigate sensing-centric (S-C) and communications-centric (C-C) designs, aiming to design DFSAC beamforming strategies that maximize SR and CR, respectively. The SR-CR region is further characterized through a Pareto optimal beamforming design. In the uplink case, we consider S-C and C-C designs, each employing distinct interference cancellation orders for S&C signals at the BS. The rate region is obtained through the time-sharing strategy between these two designs.
- We present numerical results to demonstrate that i)
  HISAC achieves higher SRs and CRs than the conventional MIMO based ISAC in both downlink and uplink
  scenarios; ii) HISAC yields more degrees of freedom
  (DoFs) than FDSAC, and the achievable SR-CR rate
  regions of FDSAC are entirely encompassed within the
  rate regions of HISAC.

The remainder of this article is organized as follows. Section II presents the conceptual framework of HISAC, including both S&C models. Then, Sections III and IV delve into the analysis of downlink and uplink S&C performance, respectively, elucidating the outcomes for both I-CSI and S-CSI. Section V provides numerical results to validate the accuracy of the derived theoretical insights. Finally, Section VI concludes the article.

Notation: Throughout this paper, scalars, vectors, and matrices are denoted by non-bold, bold lower-case, and bold

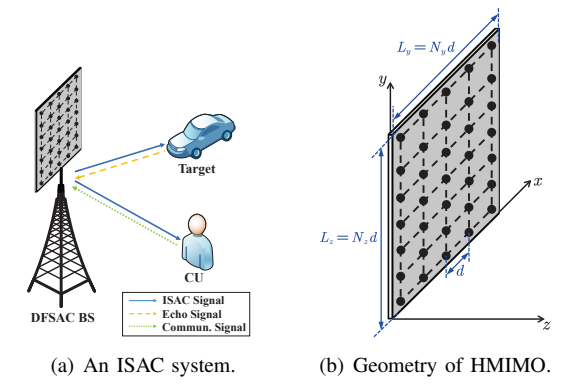


Fig. 1: Illustration of HISAC.

upper-case letters, respectively. For the matrix  $\mathbf{A}$ ,  $[\mathbf{A}]_{i,j}$ ,  $\mathbf{A}^{\mathsf{T}}$ ,  $A^*$ ,  $A^H$ , and rank (A) denote the (i, j)th entry, transpose, conjugate, transpose conjugate, and rank of A, respectively. For the square matrix  $\mathbf{B}, \mathbf{B}^{\frac{1}{2}}, \mathbf{B}^{-1}, \operatorname{tr}(\mathbf{B}), \text{ and } \det(\mathbf{B})$  denote the principal square root, inverse, trace, and determinant of B, respectively. The notation  $[\mathbf{a}]_i$  denotes the ith entry of vector a, and diag{a} returns a diagonal matrix whose diagonal elements are entries of a. The notations |a| and |a| denote the magnitude and norm of scalar a and vector  $\mathbf{a}$ , respectively. The identity matrix and zero matrix are represented by I and  $\mathbf{0}$ , respectively. The matrix inequalities  $\mathbf{A} \succeq \mathbf{0}$  imply that  $\mathbf{A}$  is positive semi-definite. The sets  $\mathbb{Z}$ ,  $\mathbb{R}$ , and  $\mathbb{C}$  stand for the integer, real, and complex spaces, respectively, and notation  $\mathbb{E}\{\cdot\}$ represents mathematical expectation. The mutual information between random variables X and Y conditioned on Z is shown by I(X;Y|Z), and  $\otimes$  denotes the Kronecker product. The modulus operator and the floor function are represented by  $\mathsf{mod}(\cdot,\cdot)$  and  $|\cdot|$ , respectively. Finally,  $\mathcal{CN}(\mu,\mathbf{X})$  is used to denote the circularly-symmetric complex Gaussian distribution with mean  $\mu$  and covariance matrix X.

#### II. SYSTEM MODEL

Consider a downlink/uplink ISAC system as depicted in Fig. 1(a), where a DFSAC BS is equipped with a HMIMO N antennas. The BS aims to serve a single-antenna communication user (CU) while simultaneously sensing a single target. As shown in Fig. 1(b), we assume that the HMIMO is deployed on the x-y plane with  $N=N_xN_y$ , where  $N_x$  and  $N_y$  denote the number of antennas along the x-axis and y-axis, respectively. The inter-element distance is denoted as d ( $d < \lambda/2$ ), where  $\lambda$  denotes the wavelength. Hence, the HMIMO has the size of  $L_x \times L_y$  with  $L_x = N_x d$  and  $L_y = N_y d$ , and centered at  $\mathbf{c} = [L_x/2, L_y/2, 0]^\mathsf{T}$ . By indexing the antennas row-byrow, the location of the nth antenna for  $n = 1, \ldots, N$  can be characterized as follows:

$$\mathbf{p}_{n} = \left[p_{n,x}, p_{n,y}, p_{n,z}\right]^{\mathsf{T}}$$

$$= \left[\operatorname{mod}\left(n - 1, N_{x}\right) d, \left\lfloor (n - 1)/N_{y} \right\rfloor d, 0\right]^{\mathsf{T}}.$$
(1)

# A. Downlink Signal Model

We commence by considering the downlink HISAC scenario, where the DFSAC signals sent by the BS are used to deliver data information to the CU and sense the environmental information at the same time. Let  $\mathbf{X} = [\mathbf{x}_1 \dots \mathbf{x}_L] \in \mathbb{C}^{N \times L}$  be a DFSAC signal sent from the BS, where L denotes the length of the communication frame/sensing pulse. From a sensing perspective,  $\mathbf{x}_\ell \in \mathbb{C}^{N \times 1}$  denotes the sensing snapshot transmitted during the  $\ell$ th time slot for  $\ell = 1, \dots, L$ . From a communication perspective,  $\mathbf{x}_\ell$  corresponds to the  $\ell$ th data symbol vector. Under the proposed HISAC framework, the downlink ISAC signal  $\mathbf{X}$  is given by

$$\mathbf{X} = \sqrt{p}\mathbf{w}\mathbf{s}^{\mathsf{H}},$$
 (2)

where  $\mathbf{w} \in \mathbb{C}^{N \times 1}$  represents the normalized beamforming vector with  $\|\mathbf{w}\|^2 = 1$ , p is the power budget, and  $\mathbf{s} = [s_1 \dots s_L]^\mathsf{H} \in \mathbb{C}^{L \times 1}$  denotes the unit-power data stream intended for the CU with  $L^{-1} \|\mathbf{s}\|^2 = 1$ .

1) Sensing Model: We assume that the target is located at  $\mathbf{r}_s = [r_{s,x}, r_{s,y}, r_{s,z}]^\mathsf{T}$ . To accurately capture the characteristics of the line-of-sight sensing links, we model the sensing links based on spherical-wave propagation, which accounts for the path loss variations across each antenna element. Let  $\mathbf{h}_s \in \mathbb{C}^{N \times 1}$  denote the sensing link between the BS and the target. The channel coefficient between the nth antenna and the target is modeled as [16]

$$\left[\mathbf{h}_{\mathbf{s}}\right]_{n} = \sqrt{\frac{\alpha_{0}}{4\pi r_{\mathbf{s}}^{2}}} e^{-\mathbf{j}k_{0} \|\mathbf{r}_{\mathbf{s}} - \mathbf{p}_{n}\|},\tag{3}$$

for  $n=1,\ldots,N$ , where  $r_{\rm s}=\|{\bf r}_{\rm s}-{\bf c}\|$  is the propagation distance,  $k_0=\frac{2\pi}{\lambda}$  is the wavenumber, and  $\alpha_0$  denotes the channel power at the reference distance 1 m.

When transmitting the DFSAC signal matrix X for target sensing, the received reflected echo signal at the BS can be written as follows:

$$\mathbf{Y}_{s} = \mathbf{G}\mathbf{X} + \mathbf{N}_{s},\tag{4}$$

where  $\mathbf{G} \in \mathbb{C}^{N \times N}$  denotes the target response matrix, and  $\mathbf{N}_{\mathrm{s}} \in \mathbb{C}^{N \times L}$  denotes the additive white Gaussian noise (AWGN) matrix with each entry having mean zero and variance  $\sigma_{\mathrm{s}}^2$ . Furthermore, the target response matrix can be modeled by the round-trip channel as follows: [17]

$$\mathbf{G} = \beta \mathbf{h}_{\mathbf{s}} \mathbf{h}_{\mathbf{s}}^{\mathsf{T}},\tag{5}$$

where  $\beta \sim \mathcal{CN}\left(0, \alpha_s\right)$  denotes the complex amplitude of the target with the average strength of  $\alpha_s$ . Substituting (2) and (5) into (4) gives

$$\mathbf{Y}_{s} = \sqrt{p}\beta \mathbf{h}_{s} \mathbf{h}_{s}^{\mathsf{T}} \mathbf{w} \mathbf{s}^{\mathsf{H}} + \mathbf{N}_{s}. \tag{6}$$

We assume that the location of the target is perfectly tracked and focus on the estimation of the reflection coefficient  $\beta$ . This sensing task aims to extract environmental information contained within  $\beta$  from the echo signal  $\mathbf{Y}_s$ , given the foreknowledge of the DFSAC signal  $\mathbf{X}$ . The information-theoretic limit for this sensing task can be quantified by the sensing mutual information (MI) that characterizes the MI between  $\mathbf{Y}_s$  and  $\beta$  conditioned on  $\mathbf{X}$  [2], [10]. On this basis, we employ the SR as the metric for sensing performance evaluation, which is defined as the sensing MI per unit time [10], [17]. Assuming that each DFSAC symbol lasts 1 unit time, the SR is written as follows:

$$\mathcal{R}_{d.s} = L^{-1}I(\mathbf{Y}_{s}; \beta|\mathbf{X}). \tag{7}$$

In particular,  $\mathcal{R}_{d,s}$  can be calculated in the following form.

**Lemma 1.** Given w, the SR can be expressed as follows:

$$\mathcal{R}_{d,s} = L^{-1} \log_2(1 + p\sigma_s^{-2} L\alpha_s \|\mathbf{h}_s\|^2 |\mathbf{h}_s^\mathsf{T} \mathbf{w}|^2). \tag{8}$$
Proof: Please refer to Appendix A for more details.

2) Communication Model: We assume that the CU is situated at a position of  $\mathbf{r}_c = [r_{c,x}, r_{c,y}, r_{c,z}]^\mathsf{T}$ . Due to the sub-half-wavelength antenna spacing in the holographic array and the presence of scatterers, spatial correlation for the small-scale fading between antennas becomes significant. Therefore, we model the communication channel response  $\mathbf{h}_c \in \mathbb{C}^{N \times 1}$  as a correlated Rayleigh-distributed vector, i.e.,  $\mathbf{h}_c \sim \mathcal{CN}\left(\mathbf{0}, \mathbf{R}\right)$ , where  $\mathbf{R} = \mathbb{E}\{\mathbf{h}_c\mathbf{h}_c^{\mathsf{H}}\} \succeq \mathbf{0}$  is the correlation matrix.

To further characterize the spatial correlation, we employ a correlation model based on the Fourier plane-wave series expansion of an electromagnetic random channel [15], which effectively captures the spatial correlation effects under scattering environment. Following the methodology in [15], the spatial impulse response  $[\mathbf{h}_{\rm c}]_n$  can be derived based on a four-dimensional (4D) Fourier plane-wave representation:

$$[\mathbf{h}_{c}]_{n} = \frac{1}{4\pi^{2}} \iiint_{\mathcal{D}\times\mathcal{D}} a_{c} (k_{x}, k_{y}, \mathbf{r}_{c}) H_{a} (k_{x}, k_{y}, \kappa_{x}, \kappa_{y})$$

$$\times a_{b} (\kappa_{x}, \kappa_{y}, \mathbf{p}_{n}) dk_{x} dk_{y} d\kappa_{x} d\kappa_{y}, \tag{9}$$

where  $\boldsymbol{\kappa} = [\kappa_x, \kappa_y, \kappa_z]^{\mathsf{T}}$  with  $\kappa_z = (k_0^2 - \kappa_x^2 - \kappa_y^2)^{\frac{1}{2}}$ ,  $\mathbf{k} = [k_x, k_y, k_z]^{\mathsf{T}}$  with  $k_z = (k_0^2 - k_x^2 - k_y^2)^{\frac{1}{2}}$ ,

$$a_{\mathbf{b}}(\kappa_x, \kappa_y, \mathbf{p}_n) = e^{-jk_0(\kappa_x p_{n,x} + \kappa_y p_{n,y} + \kappa_z p_{n,z})}, \tag{10}$$

$$a_{c}(k_{x}, k_{y}, \mathbf{r}_{c}) = e^{jk_{0}(k_{x}r_{c,x} + k_{y}r_{c,y} + k_{z}r_{c,z})}$$
 (11)

denote the transmit and receive responses at  $\mathbf{p}_n$  and  $\mathbf{r}_c$ , respectively, and the integration region  $\mathcal{D}$  is given by  $\mathcal{D} = \{(x,y) \in \mathbb{R}^2 | x^2 + y^2 \leq k_0^2\}$ . Besides,  $H_a(k_x,k_y,\kappa_x,\kappa_y)$  in (9) is referred to as the angular or wavenumber response between the transmit propagation direction  $\frac{\kappa}{\|\mathbf{k}\|}$  of the BS and the receive propagation direction  $\frac{\mathbf{k}}{\|\mathbf{k}\|}$  of the CU, which is complex Gaussian distributed with mean zero and variance determined by the scattering environment and the array geometry [15].

According to [6], [15], the channel description in (9) can be discretized via the Karhunen-Loève expansion as follows:

$$\mathbf{h}_{c} = \sqrt{N} \sum_{(m_x, m_y) \in \mathcal{E}} H(m_x, m_y) \mathbf{a}(m_x, m_y), \qquad (12)$$

where  $[\mathbf{a}(m_x,m_y)]_n = \frac{1}{\sqrt{N}}a_{\mathrm{b}}(\frac{2\pi m_x}{L_x},\frac{2\pi m_y}{L_y},\mathbf{p}_n)\mathrm{e}^{\mathrm{j}k_0r_{\mathrm{c},z}}$  for  $n=1,\ldots,N,\ \mathcal{E}=\{(m_x,m_y)\in\mathbb{Z}^2:(\frac{m_x\lambda}{L_x})^2+(\frac{m_y\lambda}{L_y})^2<1\}$ , and the set  $\{H(m_x,m_y)\sim\mathcal{CN}(0,\sigma^2(m_x,m_y))\}_{(m_x,m_y)\in\mathcal{E}}$  stores  $|\mathcal{E}|\triangleq$  n statistically independent complex Gaussian variables each with variance  $\sigma^2(m_x,m_y)$  determined by [6, Eq. (70)]. As a result,  $\mathbf{h}_{\mathrm{c}}$  can be reexpressed as follows: [15]

$$\mathbf{h}_{c} = \mathbf{U} \mathbf{\Sigma}^{\frac{1}{2}} \overline{\mathbf{h}},\tag{13}$$

where  $\overline{\mathbf{h}} \sim \mathcal{CN}(\mathbf{0}, \mathbf{I})$  contains n independently distributed Gaussian variables,  $\mathbf{\Sigma} \in \mathbb{C}^{\mathsf{n} \times \mathsf{n}}$  is a diagonal matrix whose diagonal elements are  $\{N\sigma^2(m_x,m_y)\}_{(m_x,m_y)\in\mathcal{E}}$ , and  $\mathbf{U} \in \mathbb{C}^{N \times \mathsf{n}}$  is a deterministic semi-unitary matrix collecting the n vectors  $\{\mathbf{a}(m_x,m_y)\}_{(m_x,m_y)\in\mathcal{E}}$  with  $\mathbf{U}^\mathsf{H}\mathbf{U}=\mathbf{I}$ . Based on (13), the correlation matrix  $\mathbf{R}$  can be written as follows:

$$\mathbf{R} = \mathbb{E}\left\{\mathbf{h}_{c}\mathbf{h}_{c}^{\mathsf{H}}\right\} = \mathbf{U}\boldsymbol{\Sigma}\mathbf{U}^{\mathsf{H}}.\tag{14}$$

Note that (14) can be regarded as the eigendecomposition (ED)

of  $\mathbf{R}$  with rank ( $\mathbf{R}$ ) = n and its n positive eigenvalues stored in  $\{N\sigma^2(m_x, m_y)\}_{(m_x, m_y) \in \mathcal{E}} \triangleq \{\lambda_1 \geq \ldots \geq \lambda_n > 0\}$ . The received downlink signal at the CU is given by

$$\mathbf{y}_{c}^{\mathsf{T}} = \mathbf{h}_{c}^{\mathsf{T}} \mathbf{X} + \mathbf{n}_{c}^{\mathsf{T}} = \sqrt{p} \mathbf{h}_{c}^{\mathsf{T}} \mathbf{w} \mathbf{s}^{\mathsf{H}} + \mathbf{n}_{c}^{\mathsf{T}},$$
 (15)

where  $\mathbf{n}_{\mathrm{c}} \in \mathbb{C}^{L \times 1}$  denotes the AWGN vector with each entry having mean zero and variance  $\sigma_c^2$ . Consequently, the downlink CR can be written as follows:

$$\overline{\mathcal{R}}_{d,c} = \log_2(1 + p/\sigma_c^2 |\mathbf{h}_c^\mathsf{T} \mathbf{w}|^2). \tag{16}$$

Downlink Beamforming Design: By observing (8) and (16), one can find that both the SR and CR are influenced by the beamforming vector w. However, finding an optimal w that can simultaneously maximize both the CR and SR poses a challenging task. In light of this, we will propose three beamforming designs for the downlink HISAC in Section III. The first is named the C-C (communications-centric) design, aiming to maximize the CR, while the second one is termed the S-C (sensing-centric) design, focusing on maximizing the SR. Finally, we propose a *Pareto optimal design* to characterize the Pareto boundary of the SR-CR region.

## B. Uplink Signal Model

For the uplink case, the DFSAC BS aims to extract environmental information from the reflected sensing echoes while simultaneously detecting the data symbols sent by the CU. The sensing and communication signals are assumed to be perfectly synchronized at the BS by using properly designed synchronization sequences. As a result, the BS observes the following superposed S&C signal:

$$\mathbf{Y}_{\mathrm{u}} = \sqrt{p_{\mathrm{c}}} \mathbf{h}_{\mathrm{c}} \mathbf{s}_{\mathrm{c}}^{\mathsf{H}} + \sqrt{p_{\mathrm{s}}} \mathbf{G} \mathbf{w} \mathbf{s}_{\mathrm{s}}^{\mathsf{H}} + \mathbf{N}_{\mathrm{u}}, \tag{17}$$

where  $p_{\rm c}$  is the communication power budget,  $\mathbf{s}_{\rm c} = [s_{{\rm c},1}\dots s_{{\rm c},L}]^{\rm H} \in \mathbb{C}^{L \times 1}$  denotes the message sent by the CU subject to  $\mathbb{E}\{\mathbf{s}_c\mathbf{s}_c^H\} = \mathbf{I}$ ,  $p_s$  is the sensing power budget,  $\mathbf{s}_s = [s_{s,1} \dots s_{s,L}]^H \in \mathbb{C}^{L \times 1}$  denotes the sensing pulse subject to  $L^{-1} \|\mathbf{s}_s\|^2 = 1$ , and  $\mathbf{N} \in \mathbb{C}^{N \times L}$  is the AWGN matrix with each entry having mean zero and variance  $\sigma_{ii}^2$ .

Uplink Interference Cancellation Design: To address the inter-functionality interference (IFI) between the S&C signals, the method of successive interference cancellation (SIC) with two different interference cancellation orders can be employed [10]. The first is named the S-C SIC, where the BS first detects the communication signal  $s_c$  by treating the sensing signal as interference, and then  $\sqrt{p_c}\mathbf{h_c}\mathbf{s_c^H}$  is subtracted from the superposed signal  $\mathbf{Y}_{\mathrm{u}}$ , with the remaining part utilized for sensing the target response. The second one is termed the C-C SIC, where the BS first senses the target response G by treating the communication signal as interference, and then  $\sqrt{p_{\rm s}} {\bf Gws}_{\rm s}^{\sf H}$  is subtracted from  ${\bf Y}_{\rm u}$ , with the rest part used for detecting the communication signal. Clearly, the first SIC order yields better communication performance, while the second one yields better sensing performance, which will be further discussed in Section IV.

In the context of the given HISAC framework, our aim is to assess its S&C performance in both downlink and uplink scenarios. In the following pages, we will integrate two distinct CSI assumptions into our analyses: I-CSI (instantaneous CSI) and S-CSI (statistical CSI). In the I-CSI case, the BS is assumed to possess perfect knowledge of  $h_c$ , while in the S-CSI case, the BS only has information about the distribution of  $h_c$  and its correlation matrix R.

# III. DOWNLINK PERFORMANCE ANALYSIS

In this section, we analyze the S&C performance of downlink HISAC. Specifically, the communication performance is evaluated using the ergodic CR (ECR) and OP, whereas the sensing performance is evaluated through the SR.

#### A. Instantaneous CSI

1) Sensing-Centric Design: Under the S-C design, the beamforming vector w is set to maximize the downlink SR, and the optimal beamforming vector satisfies

$$\mathbf{w} = \operatorname{argmax}_{\|\mathbf{w}\|^2 = 1} \mathcal{R}_{d,s}$$
  
= 
$$\operatorname{argmax}_{\|\mathbf{w}\|^2 = 1} |\mathbf{h}_s^\mathsf{T} \mathbf{w}|^2 = \|\mathbf{h}_s\|^{-1} \mathbf{h}_s^*.$$
(18)

By substituting  $\mathbf{w} = \|\mathbf{h}_{s}\|^{-1}\mathbf{h}_{s}^{*}$  into (8), we write the SR as follows:

$$\mathcal{R}_{d,s}^{s} = L^{-1} \log_2(1 + p\sigma_s^{-2} L\alpha_s \|\mathbf{h}_s\|^4).$$
 (19)

The following theorem provides a closed-form expression for  $\mathcal{R}_{d.s}^{s}$  as well as its high-SNR approximation.

Theorem 1. In the S-C design, the downlink SR is given by

$$\mathcal{R}_{d,s}^{s} = L^{-1} \log_2 \left( 1 + \frac{pL\alpha_s \alpha_0^2 N^2}{16\pi^2 \sigma_s^2 r_s^4} \right).$$
 (20)

When  $p \to \infty$ , the SR satisfies

$$\mathcal{R}_{d,s}^{s} \approx L^{-1} \log_2 p + L^{-1} \log_2 \left( \frac{L\alpha_s \alpha_0^2 N^2}{16\pi^2 \sigma_s^2 r_s^4} \right).$$
 (21)

*Proof:* Based on (3), we have  $\|\mathbf{h}_{s}\|^{4}$  = which yields (20). Let  $p \rightarrow \infty$  and apply the  $\lim_{x\to\infty} \frac{\log_2(1+x)}{\log_2 x} = 1$  to (20), we can obtain (21).

Remark 1. The results in Theorem 1 suggest that the high-SNR slope and power offset of the SR achieved by the S-C design are given by  $L^{-1}$  and  $\log_2\left(\frac{16\pi^2\sigma_{\rm s}^2r_{\rm s}^4}{L\alpha_{\rm s}\alpha_0^2N^2}\right)$ , respectively.

We next analyze the communication performance under the S-C design. By inserting  $\mathbf{w} = \|\mathbf{h}_{s}\|^{-1}\mathbf{h}_{s}^{*}$  into (16), we obtain the CR as follows:

$$\overline{\mathcal{R}}_{d,c}^{s} = \log_2(1 + p/\sigma_c^2 \|\mathbf{h}_s\|^{-2} |\mathbf{h}_s^{\mathsf{H}} \mathbf{h}_c|^2). \tag{22}$$

The following theorem provides a closed-form expression for the ECR  $\mathcal{R}_{d,c}^s = \mathbb{E}\{\overline{\mathcal{R}}_{d,c}^s\}$  and its high-SNR approximation.

Theorem 2. The ECR achieved by the S-C design is

$$\mathcal{R}_{d,c}^{s} = -\frac{1}{\ln 2} e^{\sigma_c^2 \Omega/p} \text{Ei}(-\sigma_c^2 \Omega/p), \qquad (23)$$

where  $\Omega=\frac{N}{\mathbf{b}^{\mathrm{H}}\mathbf{R}\mathbf{b}}$  with  $[\mathbf{b}]_n=\mathrm{e}^{-\mathrm{j}k_0\|\mathbf{r}_\mathrm{s}-\mathbf{p}_n\|}$  for  $n=1,\ldots,N,$  and  $\mathrm{Ei}\,(x)=-\int_{-x}^\infty\frac{\mathrm{e}^{-t}}{t}dt$  is the exponential integral function. When  $p\to\infty$ , the ECR satisfies

$$\mathcal{R}_{d,c}^{s} \approx \log_2 p - \log_2 \sigma_c^2 - \log_2 \Omega - \mathcal{C}/\ln 2,$$
 (24)

where C is the Euler constant.

*Proof:* Please refer to Appendix B for more details. **Remark 2.** The results in **Theorem 2** suggest that the high-SNR slope and power offset of the ECR achieved by the S-C design are given by 1 and  $\log_2(\sigma_c^2\Omega) + \frac{\mathcal{C}}{\ln 2}$ , respectively.

Furthermore, the OP of the CR is defined as follows:

$$\mathcal{P}_{d}^{s} = \Pr(\overline{\mathcal{R}}_{d,c}^{s} < \mathcal{R}_{0}), \tag{25}$$

where  $\mathcal{R}_0 > 0$  is the target rate. The following theorem provides a closed-form expression for the OP as well as its high-SNR approximation.

Theorem 3. The OP achieved by the S-C design is given by

$$\mathcal{P}_{\rm d}^{\rm s} = 1 - e^{-\sigma_{\rm c}^2 \Omega(2^{\mathcal{R}_0} - 1)/p}.$$
 (26)

When  $p \to \infty$ , the OP satisfies

$$\mathcal{P}_{\rm d}^{\rm s} \approx \sigma_{\rm c}^2 \Omega(2^{\mathcal{R}_0} - 1)/p.$$
 (27)

*Proof:* Please refer to Appendix B for more details.

**Remark 3.** The results in **Theorem 3** suggest that the diversity order and array gain of the OP achieved by the S-C design are given by 1 and  $\sigma_c^{-2}\Omega^{-1}(2^{\mathcal{R}_0}-1)^{-1}$ , respectively.

2) Communications-Centric Design: Next we focus on the C-C design. With I-CSI, the beamforming vector that maximizes the downlink CR is given by

$$\mathbf{w} = \operatorname{argmax}_{\|\mathbf{w}\|^2 = 1} \overline{\mathcal{R}}_{d,c}$$
  
= 
$$\operatorname{argmax}_{\|\mathbf{w}\|^2 = 1} |\mathbf{h}_c^\mathsf{T} \mathbf{w}|^2 = \|\mathbf{h}_c\|^{-1} \mathbf{h}_c^*.$$
 (28)

Upon substituting  $\mathbf{w} = \|\mathbf{h}_c\|^{-1}\mathbf{h}_c^*$  into (16), we express the CR as follows:

$$\overline{\mathcal{R}}_{d,c}^{c} = \log_2(1 + p/\sigma_c^2 \|\mathbf{h}_c\|^2), \tag{29}$$

A closed-form expression for the OP  $\mathcal{P}_d^c = \Pr(\overline{\mathcal{R}}_{d,c}^c < \mathcal{R}_0)$  is given as follows.

**Theorem 4.** The OP achieved by the C-C design is given by

$$\mathcal{P}_{d}^{c} = \frac{\lambda_{n}^{n}}{\prod_{n=1}^{n} \lambda_{n}} \sum_{k=0}^{\infty} \frac{\delta_{k} \Upsilon(n+k, \sigma_{c}^{2}/p\lambda_{n}^{-1}(2^{\mathcal{R}_{0}}-1))}{(n+k-1)!}, \quad (30)$$

where  $\Upsilon(s,x)=\int_0^x t^{s-1}\mathrm{e}^{-t}dt$  denotes the lower incomplete gamma function,  $\delta_0=1$ , and  $\delta_k\ (k>0)$  can be calculated recursively as  $\delta_k=\frac{1}{k}\sum_{i=1}^k\left[\sum_{n=1}^n\left(1-\lambda_n/\lambda_n\right)^i\right]\delta_{k-i}$ . When  $p\to\infty$ , the OP satisfies

$$\mathcal{P}_{d}^{c} \approx \frac{(2^{\mathcal{R}_{0}} - 1)^{n} \sigma_{c}^{2n}}{p^{n} n! \prod_{n=1}^{n} \lambda_{n}}.$$
 (31)

**Proof:** Please refer to Appendix C for more details. **Remark 4.** The results in **Theorem 4** suggest that the diversity order and array gain of the OP achieved by the C-C design are given by n and  $(n! \prod_{n=1}^{n} \lambda_n)^{\frac{1}{n}} \sigma_c^{-2} (2^{\mathcal{R}_0} - 1)^{-1}$ , respectively.

We next turn our attention to the ECR  $\mathcal{R}_{d,c}^c = \mathbb{E}\{\overline{\mathcal{R}}_{d,c}^c\}$ . Let us define

$$\zeta(\mathbf{A}, a) = \frac{\lambda_{A,r}^{r} \log_{2} e}{\prod_{r=1}^{r} \lambda_{A,r}} \sum_{k=0}^{\infty} \sum_{\mu=0}^{r+k-1} \frac{\delta_{k}}{(r+k-1-\mu)!} \times \left[ \frac{(-1)^{r+k-\mu} e^{1/a\lambda_{A,r}^{-1}}}{(a\lambda_{A,r})^{r+k-1-\mu}} \text{Ei} \left( -\frac{1}{a\lambda_{A,r}} \right) + \sum_{u=1}^{r+k-1-\mu} (u-1)! \left( -\frac{1}{a\lambda_{A,r}} \right)^{r+k-1-\mu-u} \right], (32)$$

where  $\lambda_{A,1} \geq \ldots \geq \lambda_{A,r}$  denote the positive eigenvalues of the matrix **A** with  $r = \operatorname{rank}(\mathbf{A})$ .

Theorem 5. The ECR achieved by the C-C design is

$$\mathcal{R}_{d,c}^{c} = \zeta \left( \mathbf{R}, p / \sigma_{c}^{2} \right). \tag{33}$$

When  $p \to \infty$ , the ECR satisfies

$$\mathcal{R}_{d,c}^{c} \approx \log_2 p - \log_2 \sigma_c^2 + v_{\mathbf{R}},$$
 (34)

where  $v_{\mathbf{R}} = \frac{\lambda_{\mathbf{n}}^{\mathsf{n}} \log_2 \mathbf{e}}{\prod_{n=1}^{\mathsf{n}} \lambda_n} \sum_{k=0}^{\infty} \delta_k \left( \psi(\mathbf{n} + k) + \ln(\lambda_{\mathbf{n}}) \right).$ 

*Proof:* Please refer to Appendix C for more details.

**Remark 5.** The results in **Theorem 5** suggest that the high-SNR slope and power offset of the ECR achieved by the C-C design are given by 1 and  $\log_2 \sigma_{\rm c}^2 - v_{\rm R}$ , respectively.

By substituting  $\mathbf{w} = \|\mathbf{h}_c\|^{-1}\mathbf{h}_c^*$  into (8), we obtain the SR as follows:

$$\overline{\mathcal{R}}_{d,s}^{c} = \frac{1}{L} \log_2 \left( 1 + \frac{p}{\sigma_s^2} L \alpha_s \|\mathbf{h}_s\|^2 \frac{|\mathbf{h}_c^{\mathsf{H}} \mathbf{h}_s|^2}{\|\mathbf{h}_c\|^2} \right). \tag{35}$$

To account for the statistics of  $\mathbf{h}_c$ , we define the average SR as  $\mathcal{R}_{d,s}^c \triangleq \mathbb{E}\{\overline{\mathcal{R}}_{d,s}^c\}$  to assess the sensing performance.

Theorem 6. The average SR achieved by the C-C design is

$$\mathcal{R}_{\mathrm{d}s}^{\mathrm{c}} = L^{-1}(v_{\Delta} - v_{\mathbf{R}}),\tag{36}$$

where  $v_{\Delta}$  is obtained by replacing  $\{\lambda_n\}_{n=1}^n$  in  $v_{\mathbf{R}}$  with the positive eigenvalues of  $\mathbf{\Delta} = \mathbf{R}^{\frac{1}{2}}(p/\sigma_{\mathrm{s}}^2 L \alpha_{\mathrm{s}} ||\mathbf{h}_{\mathrm{s}}||^2 \mathbf{h}_{\mathrm{s}} \mathbf{h}_{\mathrm{s}}^{\mathsf{H}} + \mathbf{I})\mathbf{R}^{\frac{1}{2}}$ . When  $p \to \infty$ , the average SR satisfies

$$\mathcal{R}_{d,s}^{c} \approx L^{-1}(\log_2 p - \log_2 \Xi - \mathcal{C}/\ln 2 - v_{\mathbf{R}}),$$
 (37)

where  $\Xi = \frac{16\pi^2 \sigma_{\rm s}^2 r_{\rm s}^4}{L\alpha_{\rm s}\alpha_{\rm o}^2 N^2} \Omega$ .

*Proof:* Please refer to Appendix D for more details.

**Remark 6.** The results in **Theorem 6** suggest that the high-SNR slope and power offset of the SR achieved by the S-C design are given by  $\frac{1}{L}$  and  $\log_2 \Xi + \frac{C}{\ln 2} + v_{\mathbf{R}}$ , respectively.

**Remark 7.** The above arguments imply that for downlink HISAC with I-CSI, the beamforming design *does not affect the high-SNR slope*, but it does *impact the diversity order*, array gain, and high-SNR power offset. Since  $n \ge 1$ , the C-C design can achieve a higher diversity order than the S-C design.

3) Pareto Optimal Design: In practical scenarios, the beamforming vector w can be customized to meet diverse quality-of-service requirements, introducing a trade-off between S&C performance. To evaluate this trade-off, we investigate the Pareto boundary of the SR-CR region. Specifically, the Pareto boundary comprises SR-CR pairs where it is impossible to enhance one of the rates without simultaneously reducing the other [18]. Any rate pair situated on this boundary can be identified by solving the following problem: [18]

$$\max_{\mathbf{w}.\mathcal{R}} \quad \mathcal{R} \tag{38a}$$

s.t. 
$$L^{-1}\log_2(1 + p/\sigma_s^2 L\alpha_s \|\mathbf{h}_s\|^2 |\mathbf{h}_s^\mathsf{T} \mathbf{w}|^2) \ge \tau \mathcal{R}$$
, (38b)

$$\log_2(1 + p/\sigma_c^2 |\mathbf{h}_c^\mathsf{T} \mathbf{w}|^2) \ge (1 - \tau)\mathcal{R},\tag{38c}$$

$$\|\mathbf{w}\|^2 = 1,\tag{38d}$$

where  $\tau \in [0,1]$  denotes a particular rate-profile parameter. The complete Pareto boundary is obtained by solving the problem (38) with  $\tau$  ranging from 0 to 1. The solution to problem (38) is given as follows.

**Theorem 7.** For a given  $\tau$ , the optimal beamforming vector

is given by

$$\mathbf{w}_{\tau} = \begin{cases} \|\mathbf{h}_{c}\|^{-1}\mathbf{h}_{c}^{*}, & \tau \in \left[0, \frac{\overline{\mathcal{R}}_{d,s}^{c}}{\overline{\mathcal{R}}_{d,c}^{c} + \overline{\mathcal{R}}_{d,s}^{c}}\right] \\ a\mathbf{h}_{1}^{*} + b\mathbf{h}_{2}^{*}e^{-j\angle\rho}, & \tau \in \left(\frac{\overline{\mathcal{R}}_{d,s}^{c}}{\overline{\mathcal{R}}_{d,c}^{c} + \overline{\mathcal{R}}_{d,s}^{c}}, \frac{\mathcal{R}_{d,s}^{s}}{\overline{\mathcal{R}}_{d,c}^{s} + \mathcal{R}_{d,s}^{s}}\right). \\ \|\mathbf{h}_{s}\|^{-1}\mathbf{h}_{s}^{*}, & \tau \in \left[\frac{\mathcal{R}_{d,s}^{s}}{\overline{\mathcal{R}}_{d,c}^{s} + \mathcal{R}_{d,s}^{s}}, 1\right] \end{cases}$$

$$(39)$$

where  $\mathbf{h}_1 = \sqrt{p/\sigma_{\mathrm{c}}^2} \mathbf{h}_{\mathrm{c}}$ ,  $\mathbf{h}_2 = \sqrt{\frac{p\alpha_0 L\alpha_s N}{4\pi\sigma_{\mathrm{s}}^2 r_{\mathrm{s}}^2}} \mathbf{h}_{\mathrm{s}}$ ,  $\rho = \mathbf{h}_1^{\mathrm{H}} \mathbf{h}_2$ ,  $a = \frac{\mu_1 \sqrt{2^{(1-\tau)\mathcal{R}^\star} - 1}}{\eta}$  and  $b = \frac{\mu_2 \sqrt{2^{\tau L\mathcal{R}^\star} - 1}}{\eta}$  with  $\eta$  for normalization,  $\mu_1 = \frac{\xi_2}{\chi}$  and  $\mu_2 = \frac{\xi_1}{\chi}$  with  $\xi_1 = \|\mathbf{h}_1\|^2 - \sqrt{\frac{2^{(1-\tau)\mathcal{R}^\star} - 1}{2^{\tau L\mathcal{R}^\star} - 1}} |\rho|$ ,  $\xi_2 = \|\mathbf{h}_2\|^2 - \sqrt{\frac{2^{\tau L\mathcal{R}^\star} - 1}{2^{(1-\tau)\mathcal{R}^\star} - 1}} |\rho|$ , and  $\chi = \xi_1 2^{\tau L\mathcal{R}^\star} \tau L \ln 2 + \xi_2 2^{(1-\tau)\mathcal{R}^\star} (1-\tau) \ln 2$ .  $\mathcal{R}^\star$  denotes the solution to the equation  $\xi_1 (2^{\tau L\mathcal{R}} - 1) + \xi_2 (2^{(1-\tau)\mathcal{R}} - 1) = \|\mathbf{h}_1\|^2 \|\mathbf{h}_2\|^2 - |\rho|^2$ .

**Proof:** Please refer to Appendix E for more details. **Remark 8.** The results in **Theorem 7** suggest that the Pareto optimal beamforming vector lies in the plane spanned by  $\mathbf{h}_c^*$  and  $\mathbf{h}_s^* e^{-j \angle \rho}$ .

Given au, let  $\mathcal{R}_{d,s}^{ au}$  and  $\mathcal{R}_{d,c}^{ au}$  denote the SR and the CR achieved by Pareto optimal beamforming vector  $\mathbf{w}_{ au}$ , respectively. Accordingly, we have  $\mathcal{R}_{d,s}^{ au} \in [\overline{\mathcal{R}}_{d,s}^c, \mathcal{R}_{d,s}^s]$  and  $\mathcal{R}_{d,c}^{ au} \in [\overline{\mathcal{R}}_{d,c}^s, \overline{\mathcal{R}}_{d,c}^s]$  with  $\mathcal{R}_{d,s}^0 = \overline{\mathcal{R}}_{d,s}^c, \mathcal{R}_{d,s}^1 = \mathcal{R}_{d,s}^s, \mathcal{R}_{d,c}^0 = \overline{\mathcal{R}}_{d,c}^c$  and  $\mathcal{R}_{d,c}^1 = \overline{\mathcal{R}}_{d,c}^s$ . By exploiting the Sandwich theorem, the high-SNR slopes and diversity orders of any SR-CR pair on the Pareto boundary can be obtained. Finally, letting  $(\mathcal{R}_s, \mathcal{R}_c)$  denote the achievable SR-CR pair, the SR-CR region achieved by HISAC with I-CSI can be written as follows:

$$\mathcal{C}_{d} = \left\{ (\mathcal{R}_{s}, \mathcal{R}_{c}) \middle| \mathcal{R}_{s} \in [0, \mathcal{R}_{d,s}^{\tau}], \mathcal{R}_{c} \in [0, \mathcal{R}_{d,c}^{\tau}], \tau \in [0, 1] \right\}. \tag{40}$$

#### B. Statistical CSI

Having investigated the I-CSI case, we now move to the S-CSI case where the BS has no knowledge of  $\mathbf{h}_c$  and only knows  $\mathbf{R}$ .

- 1) Sensing-Centric Design: Since the optimal beamforming vector under the S-C design, i.e.,  $\|\mathbf{h}_{\mathrm{s}}\|^{-1}\mathbf{h}_{\mathrm{s}}^*$ , is independent of  $\mathbf{h}_{\mathrm{c}}$ , the S&C performance of the S-C design in the S-CSI case is the same as that in the I-CSI case.
- 2) Communications-Centric Design: Since the instantaneous information of  $\mathbf{h}_{c}$  is unknown to the BS, the C-C beamforming vector is set to maximize the ECR instead of the instantaneous CR. As a result, the optimal beamforming vector satisfies

$$\mathbf{w} = \operatorname{argmax}_{\|\mathbf{w}\|^2 = 1} \mathbb{E}\{\overline{\mathcal{R}}_{d,c}\}$$
 (41)

$$= \operatorname{argmax}_{\|\mathbf{w}\|^2 = 1} \mathbb{E}\{\log_2(1 + p/\sigma_c^2 |\mathbf{h}_c^\mathsf{T}\mathbf{w}|^2)\}. \tag{42}$$

The solution to the above problem is summarized as follows. **Lemma 2.** The optimal beamforming vector under the C-C design with S-CSI is given by the normalized principal eigenvector of  $\mathbf{R}$ , i.e.,  $\mathbf{a}(m_x^{\star}, m_y^{\star}) \triangleq \mathbf{a}_{\star}$ , where

$$(m_x^{\star}, m_y^{\star}) = \operatorname{argmax}_{(m_x, m_y) \in \mathcal{E}} \sigma^2(m_x, m_y). \tag{43}$$

*Proof:* Please refer to Appendix F for more details.

By setting  $\mathbf{w} = \mathbf{a}_{\star}$ , we obtain

$$\mathbf{a}_{\star}^{\mathsf{H}} \mathbf{R} \mathbf{a}_{\star} = \max_{(m_x, m_y) \in \mathcal{E}} \sigma^2(m_x, m_y) = \lambda_1.$$
 (44)

We then present the analytical results for the ECR and OP in the following theorems.

**Theorem 8.** With S-CSI, the ECR achieved by the C-C design can be written as follows:

$$\mathcal{R}_{d,c}^{c} = -e^{\sigma_{c}^{2} \lambda_{1}^{-1}/p} \text{Ei}(-\sigma_{c}^{2} \lambda_{1}^{-1}/p) \log_{2} e.$$
 (45)

When  $p \to \infty$ , the ECR satisfies

$$\mathcal{R}_{d,c}^{c} \approx \log_2 p - \log_2 \sigma_c^2 + \log_2 \lambda_1 - \mathcal{C}/\ln 2.$$
 (46)

**Theorem 9.** With S-CSI, the OP achieved by the C-C design can be written as follows:

$$\mathcal{P}_{d}^{c} = 1 - e^{-\sigma_{c}^{2} \lambda_{1}^{-1} (2^{\mathcal{R}_{0}} - 1)/p}.$$
 (47)

When  $p \to \infty$ , the OP satisfies

$$\mathcal{P}_{d}^{c} \approx \sigma_{c}^{2} \lambda_{1}^{-1} (2^{\mathcal{R}_{0}} - 1)/p. \tag{48}$$

*Proof:* Similar to the proof of **Theorem 3**.

**Remark 9.** The results in **Theorem 8** and **9** suggest that the high-SNR slope and diversity order of the CR achieved by the C-C design with S-CSI are both equal to 1.

In the sequel, we analyze the SR achieved by the C-C design under the S-CSI case.

**Theorem** 10. Let us define  $\Gamma \triangleq \frac{L\alpha_s\alpha_0^2N}{16\pi^2r_*^4}|\sum_{n=1}^N a_{\rm b}^*(\frac{2\pi m_x}{L_x},\frac{2\pi m_y}{L_y},\mathbf{p}_n)\mathrm{e}^{-\mathrm{j}k_0r_{c,z}-\mathrm{j}k_0}\|\mathbf{r}_{\rm s}-\mathbf{p}_n\||^2.$  The SR achieved by the C-C design with S-CSI can be written as follows:

$$\mathcal{R}_{d,s}^{c} = L^{-1} \log_2 \left( 1 + p/\sigma_s^2 \Gamma \right), \tag{49}$$

When  $p \to \infty$ , the SR satisfies

$$\mathcal{R}_{d,s}^{c} \approx L^{-1} \log_2 p + L^{-1} \log_2(\Gamma/\sigma_s^2).$$
 (50)

**Remark 10.** The results in **Theorem 10** suggest that the high-SNR slope and power offset of the SR achieved by the C-C design with S-CSI are given by 1/L and  $\log_2(\sigma_{\rm s}^2/\Gamma)$ , respectively.

In addition to this, the following conclusion can be found.

**Remark 11.** The above arguments imply that for downlink HISAC with S-CSI, the beamforming design *does not affect the high-SNR slope and diversity order*, but it does *impact the array gain and high-SNR power offset*. Specifically, under the C-C design, the diversity order achieved with I-CSI is higher than that achieved with S-CSI.

3) Pareto Optimal Design: We next characterize the downlink rate region in the case of S-CSI. Based on the proof in Appendix F, the ECR  $\mathbb{E}\{\overline{\mathcal{R}}_{d,c}\}$  is monotonically increasing with  $\mathbf{w}^T\mathbf{R}\mathbf{w}^*$ . As a result, the rate region can be characterized by first solving the following problem:

$$\max x$$
 (51a)

s.t. 
$$\mathbf{w}^\mathsf{T} \mathbf{R} \mathbf{w}^* > (1 - \tau) x$$
,  $|\mathbf{h}_s^\mathsf{T} \mathbf{w}|^2 > \tau x$ , (51b)

$$\|\mathbf{w}\|^2 = 1,\tag{51c}$$

for  $\tau \in [0, 1]$ , and then calculating the corresponding SR-ECR pair. By defining  $\mathbf{W} \triangleq \mathbf{w}^* \mathbf{w}^\mathsf{T}$  and  $\mathbf{H} \triangleq \mathbf{h}_{\mathbf{s}} \mathbf{h}_{\mathbf{s}}^\mathsf{H}$ , problem (51)

	Sensing		Communications			
Design	I-CSI	S-CSI	I-CSI		S-CSI	
	$\mathcal S$	$\mathcal S$	$\mathcal{S}$	$\mathcal{D}$	$\mathcal{S}$	$\mathcal{D}$
S-C	1/L	1/L	1	1	1	1
C-C	1/L	1/L	1	n	1	1
Pareto Optimal	1/L	1/L	1	[1, n]	1	1
FDSAC	$(1-\kappa)/L$	$(1-\kappa)/L$	κ	n	κ	1

TABLE I: Downlink High-SNR Slope (S) and Diversity Order (D) with I-CSI and S-CSI

can be rewritten as follows:

$$\max_{\mathbf{W},x} x \tag{52a}$$

s.t. 
$$\operatorname{tr}(\mathbf{RW}) > (1 - \tau)x$$
,  $\operatorname{tr}(\mathbf{HW}) > \tau x$ , (52b)

$$tr(\mathbf{W}) = 1, \ \mathbf{W} \succeq \mathbf{0}, \ rank(\mathbf{W}) = 1,$$
 (52c)

which is a non-convex problem whose optimal solution generally requires a brute-force search. Let  $(\mathcal{R}_{d,s}^{\tau},\mathcal{R}_{d,c}^{\tau})$  denote the optimal SR-CR pair corresponding to  $\tau$ . Then the high-SNR slopes and diversity orders of  $(\mathcal{R}_{d,s}^{\tau},\mathcal{R}_{d,c}^{\tau})$  can be derived by using the Sandwich theorem. Besides, the rate region can be characterized as follows:

$$\mathcal{C}_{d} = \left\{ (\mathcal{R}_{s}, \mathcal{R}_{c}) \middle| \mathcal{R}_{s} \in [0, \mathcal{R}_{d,s}^{\tau}], \mathcal{R}_{c} \in [0, \mathcal{R}_{d,c}^{\tau}], \tau \in [0, 1] \right\}. \tag{53}$$

Unfortunately, obtaining the entire rate region is computationally inefficient. As a compromise, we next provide an inner bound of the rate region. The non-convexity of (52) lies in the rank-one constraint  $\operatorname{rank}(\mathbf{W})=1$ . For this constraint, the conventional approach is applying semidefinite relaxation (SDR), where we first solve the problem by ignoring the rank-one constraint, and then construct a rank-one solution with Gaussian randomization method if the solution obtained from the relaxed problem is not rank-one [19]. Let  $\overline{\mathcal{C}}_{\rm d}$  denote the SR-CR region achieved by the SDR-based method. Then we have  $\overline{\mathcal{C}}_{\rm d}\subseteq \mathcal{C}_{\rm d}$ . The boundary of  $\overline{\mathcal{C}}_{\rm d}$  thus serves an inner bound for  $\overline{\mathcal{C}}_{\rm d}$ , whose tightness will be verified by the numerical results presented in Section V.

#### C. HMIMO Based FDSAC

We consider HMIMO based FDSAC, referred to as FDSAC for simplicity, as a baseline scenario, where  $\kappa \in [0,1]$  fraction of the total bandwidth and  $\iota \in [0,1]$  fraction of the total power is used for communications, and the other is used for sensing. Consequently, the SR achieved by FDSAC is given by  $\mathcal{R}_{\rm d,s}^{\rm f} = \frac{1-\kappa}{L}\log_2(1+\frac{1-\iota}{1-\kappa}p/\sigma_{\rm s}^2L\alpha_{\rm s}\|\mathbf{h}_{\rm s}\|^4).$  As for communications, the CRs in the cases of I-CSI and S-CSI can be written as  $\mathcal{R}_{\rm d,c}^{\rm f} = \kappa\log_2(1+\frac{\iota}{\kappa}p/\sigma_{\rm c}^2\|\mathbf{h}_{\rm c}\|^2)$  and  $\mathcal{R}_{\rm d,c}^{\rm f} = \kappa\log_2(1+\frac{\iota}{\kappa}p/\sigma_{\rm c}^2\|\mathbf{h}_{\rm c}\|^2)$ , respectively. Note that the CR and SR achieved by FDSAC can be analyzed in a similar way we analyze those achieved by HISAC. For the sake of reference, we summarize the results related to diversity order and high-SNR slope in Table I.

**Remark 12.** The results in Table I indicate that HISAC can achieve higher high-SNR slopes for both downlink SR and CR than FDSAC, providing more DoFs in terms of both S&C.

Moreover, the SR-CR region of downlink FDSAC satisfies

$$C_{d}^{f} = \left\{ (\mathcal{R}_{s}, \mathcal{R}_{c}) \middle| \begin{matrix} \mathcal{R}_{s} \in [0, \mathcal{R}_{d,s}^{f}], \mathcal{R}_{c} \in [0, \mathcal{R}_{d,c}^{f}], \\ \kappa \in [0, 1], \iota \in [0, 1] \end{matrix} \right\}.$$
 (54)

#### IV. UPLINK PERFORMANCE ANALYSIS

Having analyzed the downlink performance of HISAC, we now shift our fucus on the uplink performance.

#### A. Instantaneous CSI

1) Communications-Centric SIC: Let us first study the sensing performance achieved by the C-C SIC, where the target response signal is firstly estimated by regarding the communication signal as interference. From a worst-case design perspective, we can treat the aggregate interference-plus-noise  $\mathbf{Z}_c = \sqrt{p_c}\mathbf{h}_c\mathbf{s}_c^H + \mathbf{N}_u$  as the Gaussian noise [20]. Under this consideration, we conclude the following lemma.

**Lemma 3.** The SR achieved by the C-C SIC is given by

$$\overline{\mathcal{R}}_{\mathrm{u,s}}^{\mathrm{c}} = \frac{1}{L} \log_2 \left[ 1 + \frac{p_{\mathrm{s}} L \alpha_{\mathrm{s}} |\mathbf{h}_{\mathrm{s}}^{\mathsf{T}} \mathbf{w}|^2}{\sigma_{\mathrm{u}}^2} \left( \|\mathbf{h}_{\mathrm{s}}\|^2 - \frac{p_{\mathrm{c}} |\mathbf{h}_{\mathrm{s}}^{\mathsf{H}} \mathbf{h}_{\mathrm{c}}|^2}{p_{\mathrm{c}} \|\mathbf{h}_{\mathrm{c}}\|^2 + \sigma_{\mathrm{u}}^2} \right) \right]. \tag{55}$$

*Proof:* Please refer to Appendix G for more details. The results in **Lemma 3** suggest that the SR is maximized when  $\mathbf{w} = \|\mathbf{h}_{\mathrm{s}}\|^{-1}\mathbf{h}_{\mathrm{s}}^*$ . The following theorem provide a closed-form expression for the average SR  $\mathcal{R}_{\mathrm{u,s}}^{\mathrm{c}} = \mathbb{E}\{\overline{\mathcal{R}}_{\mathrm{u,s}}^{\mathrm{c}}\}$  and its high-SNR approximation.

Theorem 11. The average SR achieved by the C-C SIC is

$$\mathcal{R}_{\mathrm{u,s}}^{c} = \frac{1}{L} \left[ \zeta \left( \boldsymbol{\Theta}, \frac{p_{\mathrm{c}}}{\sigma_{\mathrm{u}}^{2}} \boldsymbol{\Psi}^{-1} \right) - \zeta \left( \mathbf{R}, \frac{p_{\mathrm{c}}}{\sigma_{\mathrm{u}}^{2}} \right) + \log_{2} \boldsymbol{\Psi} \right], \quad (56)$$
 where  $\boldsymbol{\Theta} = \mathbf{R} + \frac{p_{\mathrm{s}}}{\sigma_{\mathrm{u}}^{2}} L \alpha_{\mathrm{s}} \| \mathbf{h}_{\mathrm{s}} \|^{2} \, \mathbf{R}^{\frac{1}{2}} (\| \mathbf{h}_{\mathrm{s}} \|^{2} \, \mathbf{I}_{N} - \mathbf{h}_{\mathrm{s}} \mathbf{h}_{\mathrm{s}}^{\mathsf{H}}) \mathbf{R}^{\frac{1}{2}} \succeq \mathbf{0},$  and  $\boldsymbol{\Psi} = \frac{p_{\mathrm{s}}}{\sigma_{\mathrm{u}}^{2}} L \alpha_{\mathrm{s}} \| \mathbf{h}_{\mathrm{s}} \|^{4} + 1.$  When  $p_{\mathrm{s}} \rightarrow \infty$ , its high-SNR approximation satisfies

$$\mathcal{R}_{\mathrm{u,s}}^{\mathrm{c}} \approx \frac{1}{L} \left[ \log_2 p_{\mathrm{s}} + \zeta \left( \tilde{\mathbf{\Theta}}, \frac{p_{\mathrm{c}}}{\sigma_{\mathrm{u}}^2 \tilde{\boldsymbol{\Psi}}} \right) - \zeta \left( \mathbf{R}, \frac{p_{\mathrm{c}}}{\sigma_{\mathrm{u}}^2} \right) + \log_2 \tilde{\boldsymbol{\Psi}} \right], \quad (57)$$
where  $\tilde{\mathbf{\Theta}} = L\alpha_{\mathrm{s}} \|\mathbf{h}_{\mathrm{s}}\|^2 \mathbf{R}^{\frac{1}{2}} (\|\mathbf{h}_{\mathrm{s}}\|^2 \mathbf{I}_N - \mathbf{h}_{\mathrm{s}} \mathbf{h}_{\mathrm{s}}^{\mathsf{H}}) \mathbf{R}^{\frac{1}{2}}, \quad \text{and} \quad \tilde{\boldsymbol{\Psi}} = L\alpha_{\mathrm{s}} \|\mathbf{h}_{\mathrm{s}}\|^4 / \sigma_{\mathrm{u}}^2.$ 

**Proof:** Similar to the proof of **Theorem 6**. **Remark 13. Theorem 11** suggests that the high-SNR slope of the SR achieved by the C-C SIC is given by 1/L.

After estimating the target response, the echo signal  $\sqrt{p_s}\mathbf{G}\mathbf{w}\mathbf{s}_s^\mathsf{H}$  can be removed from the received superposed S&C signal. The remaining communication signal is then decoded using the optimal detection vector  $\|\mathbf{h}_c\|^{-1}\mathbf{h}_c$ . Consequently, the CR is given by  $\overline{\mathcal{R}}_{u,c}^c = \log_2(1 + \frac{p_c}{\sigma_u^2}\|\mathbf{h}_c\|^2)$ . In this scenario, the ECR  $\mathcal{R}_{u,c}^c = \mathbb{E}\{\overline{\mathcal{R}}_{u,c}^c\}$  and the OP  $\mathcal{P}_u^c = \Pr(\overline{\mathcal{R}}_{u,s}^c < \mathcal{R}_0)$  can be analyzed in a similar way we analyze those achieved by the downlink C-C design with I-CSI. Further details are omitted for brevity.

2) Sensing-Centric SIC: In the context of S-C SIC, the BS first detects the communication signal from the CU, considering the echo signal  $\sqrt{p_{\rm s}} \mathbf{Gws}_{\rm s}^{\rm H}$  as interference. From a worst-case design perspective, the aggregate interference-plusnoise  $\mathbf{Z}_{\rm s} = \sqrt{p_{\rm s}} \mathbf{Gws}_{\rm s}^{\rm H} + \mathbf{N}_{\rm u}$  is treated as the Gaussian noise [20]. Under this circumstance, the uplink ECR and OP are given in the following theorems, respectively.

**Theorem 12.** The uplink ECR of the S-C design is given by

$$\mathcal{R}_{\mathrm{u.c}}^{\mathrm{s}} = \zeta(\mathbf{\Phi}, p_{\mathrm{c}}/\sigma_{\mathrm{u}}^{2}),\tag{58}$$

where  $\mathbf{\Phi} = \mathbf{R}^{\frac{1}{2}}(p_{\rm s}/\sigma_{\rm u}^2\alpha_{\rm s}\|\mathbf{h}_{\rm s}\|^2\mathbf{h}_{\rm s}\mathbf{h}_{\rm s}^{\sf H}+\mathbf{I})^{-1}\mathbf{R}^{\frac{1}{2}}\succeq\mathbf{0}$ . When  $p_{\rm c}\to\infty$ , the ECR satisfies

$$\mathcal{R}_{\text{u.c}}^{\text{s}} \approx \log_2 p_{\text{c}} - \log_2 \sigma_{\text{u}}^2 + v_{\mathbf{\Phi}},\tag{59}$$

where  $v_{\Phi}$  is obtained by replacing  $\{\lambda_n\}_{n=1}^n$  in  $v_{\mathbf{R}}$  with the positive eigenvalues of  $\Phi$ .

*Proof:* Please refer to Appendix H for more details.

**Theorem 13.** The OP achieved by the S-C SIC is written as

$$\mathcal{P}_{\mathbf{u}}^{\mathbf{s}} = \frac{\lambda_{\Phi,\mathbf{m}}^{\mathbf{m}}}{\prod_{m=1}^{\mathbf{m}} \lambda_{\Phi,m}} \sum_{k=0}^{\infty} \frac{\delta_k' \Upsilon\left(\mathbf{m} + k, \sigma_{\mathbf{u}}^2 / p_{\mathbf{c}} \lambda_{\Phi,\mathbf{m}}^{-1}(2^{\mathcal{R}_0} - 1)\right)}{(\mathbf{m} + k - 1)!},$$
(60)

where  $\lambda_{\Phi,1} \geq \ldots \geq \lambda_{\Phi,m}$  denote the positive eigenvalues of the matrix  $\Phi$  with  $\mathbf{m} = \mathrm{rank}(\Phi) \leq N$ ,  $\delta_0' = 1$ , and  $\delta_k'$  (k > 0) can be obtained recursively by  $\delta_k' = \frac{1}{k} \sum_{i=1}^k \left[ \sum_{m=1}^m \left( 1 - \lambda_{\Phi,m} / \lambda_{\Phi,m} \right)^i \right] \delta_{k-i}'$ . When  $p_c \to \infty$ , the OP satisfies

$$\mathcal{P}_{\mathbf{u}}^{\mathbf{s}} \approx \frac{(2^{\mathcal{R}_0} - 1)^{\mathsf{m}} \sigma_{\mathbf{u}}^{2\mathsf{m}}}{p_{\mathbf{c}}^{\mathsf{m}} \mathsf{m}! \prod_{m=1}^{\mathsf{m}} \lambda_{\Phi, m}}.$$
 (61)

*Proof:* Similar to the proof of **Theorem 4**.

**Remark 14.** The results in **Theorem 13** suggest that the diversity order and array gain of the OP achieved by the S-C sic are given by m and  $(m! \prod_{m=1}^{m} \lambda_{\Phi,m})^{\frac{1}{m}} \sigma_{\mathrm{u}}^{-2} (2^{\mathcal{R}_0} - 1)^{-1}$ , respectively.

After detecting the communication signal, the BS subtracts it from the received signal, utilizing the remaining part to extract information from the target response matrix G, which yields a same SR as in **Theorem 1**, i.e.,  $\mathcal{R}_{u.s}^s = \mathcal{R}_{d.s}^s$ .

**Remark 15.** For the uplink scenario with I-CSI, the SIC order does not affect the high-SNR slopes of both the CR and SR, whereas it does affect the diversity order and high-SNR slope. Specifically, since  $m = \operatorname{rank}(\Phi) \leq \operatorname{rank}(\mathbf{R}) = n$ , the diversity order achieved by the C-C SIC is no smaller than that achieved by the S-C SIC.

#### B. Statistic CSI

Having investigated the S&C performance in the case of I-CSI, we shift our focus to the case of S-CSI. In this scenario, the BS lacks complete knowledge of the communication channel  $\mathbf{h}_c$ . Consequently, the BS can only utilize the S-CSI to design the detection vector for the communication signal, which is denoted as  $\mathbf{v}$ . It is assumed that the BS possesses knowledge of the effective channel  $\mathbf{v}^H\mathbf{h}_c \in \mathbb{C}$ , the acquisition of which incurs significantly lower signaling overhead than obtaining  $\mathbf{h}_c$ .

1) Communications-Centric SIC: We commence by analyzing the SR achieved by the C-C SIC.

**Theorem 14.** By treating  $\mathbf{Z}_c$  as Gaussian noise, the SR is given by

$$\mathcal{R}_{\mathrm{u,s}}^{\mathrm{c}} = L^{-1} \log_2 \left( 1 + p_{\mathrm{s}} L \alpha_{\mathrm{s}} \|\mathbf{h}_{\mathrm{s}}\|^2 \mathbf{h}_{\mathrm{s}}^{\mathsf{H}} \left( p_{\mathrm{c}} \mathbf{R} + \sigma_{\mathrm{u}}^2 \mathbf{I} \right)^{-1} \mathbf{h}_{\mathrm{s}} \right). \tag{62}$$

When  $p_s \to \infty$ , the SR satisfies

$$\mathcal{R}_{\mathbf{u},\mathbf{s}}^{\mathbf{c}} \approx L^{-1} \log_2 p_{\mathbf{s}} + L^{-1} \log_2 (L\alpha_{\mathbf{s}} \|\mathbf{h}_{\mathbf{s}}\|^2 \mathbf{h}_{\mathbf{s}}^{\mathsf{H}} (p_{\mathbf{c}} \mathbf{R} + \sigma_{\mathbf{u}}^2 \mathbf{I})^{-1} \mathbf{h}_{\mathbf{s}}).$$
(63)

*Proof:* Similar to the proof of **Theorem 11**.

**Remark 16. Theorem 14** suggests that the high-SNR slope of the SR achieved by the C-C SIC is given by  $L^{-1}$ .

After estimating the target response, the echo signal can be removed from  $\mathbf{Y}_u$  with the remaining communication signal being without interference. The resulting ECR  $\mathcal{R}_{u,c}^c$  and OP can thus be analyzed by following similar steps shown in **Theorem 8** and **9**, respectively.

2) Sensing-Centric SIC: Then we move to the S-C design where the communication signal is first detected by considering the echo signal as interference. Under the S-C design, the uplink CR is written as follows:

$$\overline{\mathcal{R}}_{u,c}^{s} = \log_2 \left( 1 + \frac{p_c |\mathbf{v}^{\mathsf{H}} \mathbf{h}_c|^2}{p_s \alpha_s ||\mathbf{h}_s||^2 |\mathbf{v}^{\mathsf{H}} \mathbf{h}_s|^2 + \sigma_u^2} \right), \tag{64}$$

where  ${\bf v}$  denotes the communication detection vector with  $\|{\bf v}\|^2=1$ . Recalling that the BS only has the statistical information of  ${\bf h}_c$ ,  ${\bf v}$  should be designed to maximize the ECR  ${\cal R}^s_{u,c}={\mathbb E}\{\overline{\cal R}^s_{u,c}\}$ . The following lemma gives the optimal detection vector that maximizes the ECR.

**Lemma 4.** The optimal detection vector under the S-C design with S-CSI is given by

$$\mathbf{v}_{\star} = \frac{(p_{s}/\sigma_{u}^{2}\alpha_{s} \|\mathbf{h}_{s}\|^{2} \mathbf{h}_{s}\mathbf{h}_{s}^{\mathsf{H}} + \mathbf{I})^{-\frac{1}{2}}\mathbf{u}_{\star}}{\mathbf{u}_{\star}^{\mathsf{H}}(p_{s}/\sigma_{u}^{2}\alpha_{s} \|\mathbf{h}_{s}\|^{2} \mathbf{h}_{s}\mathbf{h}_{s}^{\mathsf{H}} + \mathbf{I})^{-1}\mathbf{u}_{\star}},$$
(65)

 $\begin{array}{ll} \text{where} \quad \mathbf{u}_{\star} \quad \text{is} \quad \text{the principal eigenvector of} \\ \left(p_{s}/\sigma_{u}^{2}\alpha_{s} \left\|\mathbf{h}_{s}\right\|^{2} \mathbf{h}_{s}\mathbf{h}_{s}^{\mathsf{H}} + \mathbf{I}\right)^{-\frac{1}{2}}\mathbf{R}(p_{s}/\sigma_{u}^{2}\alpha_{s} \left\|\mathbf{h}_{s}\right\|^{2} \mathbf{h}_{s}\mathbf{h}_{s}^{\mathsf{H}} + \mathbf{I})^{-\frac{1}{2}}. \end{array}$ 

*Proof:* Please refer to Appendix I for more details.

By setting  $\mathbf{v}=\mathbf{v}_{\star}$ , the communication performance is studied in the following theorems.

**Theorem 15.** The uplink ECR achieved by the S-C design is derived as

$$\mathcal{R}_{\mathrm{u,c}}^{\mathrm{s}} = -\frac{1}{\ln 2} e^{\frac{\sigma_{\mathrm{u}}^2}{p_{\mathrm{c}}\varkappa}} \mathrm{Ei}(-\frac{\sigma_{\mathrm{u}}^2}{p_{\mathrm{c}}\varkappa}). \tag{66}$$

When  $p_c \to \infty$ , the ECR satisfies

$$\mathcal{R}_{\mathrm{u,c}}^{\mathrm{s}} \approx \log_2 p_{\mathrm{c}} - \log_2 \sigma_{\mathrm{u}}^2 + \log_2 \varkappa - \mathcal{C} \log_2 e.$$
 (67)

*Proof:* Similar to the proof of **Theorem 2**.

**Theorem 16.** The OP of the S-C design is given by

$$\mathcal{P}_{u}^{s} = 1 - e^{-\frac{\sigma_{u}^{2}(2^{\mathcal{R}_{0}} - 1)}{p_{c} \varkappa}}.$$
 (68)

When  $p_c \to \infty$ , the OP satisfies

$$\tilde{\mathcal{P}}_{\mathbf{u}}^{\mathbf{s}} \approx \frac{\sigma_{\mathbf{u}}^{2}(2^{\mathcal{R}_{0}} - 1)}{p_{c}\varkappa}.$$
(69)

*Proof:* Similar to the proof of **Theorem 3**.

**Remark 17.** The results in **Theorem 15** and **16** suggest that the high-SNR slope and diversity order of the CR achieved by the S-C SIC with S-CSI are both equal to 1.

After decoding the communication signal, the sensing information can be estimated without interference, which yields a same average SR as in **Theorem 1**, i.e.,  $\mathcal{R}_{u.s}^s = \mathcal{R}_{d.s}^s$ .

Based on the analysis above for the uplink HISAC, we can make the following conclusion.

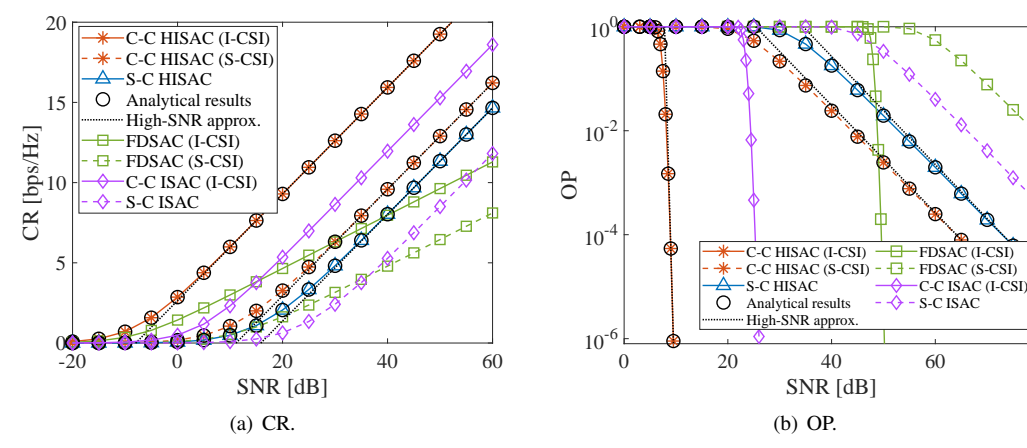


Fig. 2: Downlink communication performance.

	Sensing		Communications			
Design	I-CSI	S-CSI	I-CSI		S-CSI	
	${\mathcal S}$	${\mathcal S}$	$\mathcal{S}$	$\mathcal{D}$	$\mathcal{S}$	$\mathcal{D}$
S-C	1/L	1/L	1	m	1	1
C-C	1/L	1/L	1	n	1	1
Time-Sharing	1/L	1/L	1	[m, n]	1	1
FDSAC	$(1-\kappa)/L$	$(1-\kappa)/L$	$\kappa$	n	$\kappa$	1

TABLE II: Uplink High-SNR Slope (S) and Diversity Order (D) with I-CSI and S-CSI

**Remark 18.** For the uplink scenario with S-CSI, the SIC order does not affect either the high-SNR slopes or diversity orders. Besides, I-CSI yields higher diversity orders than S-CSI.

## C. Rate Region Characterization

To characterize the uplink SR-CR region, we utilize the time-sharing strategy [21], where the S-C SIC is applied with probability  $\epsilon$  and the C-C SIC is applied with probability  $1-\epsilon$ . For a given  $\epsilon$ , letting  $(\mathcal{R}^{\epsilon}_{\mathrm{u,s}},\mathcal{R}^{\epsilon}_{\mathrm{u,c}})$  represent the achievable SR-CR pair, we have  $\mathcal{R}^{\epsilon}_{\mathrm{u,s}} = \epsilon \mathcal{R}^{\mathrm{S}}_{\mathrm{u,s}} + (1-\epsilon)\mathcal{R}^{\mathrm{c}}_{\mathrm{u,s}}$  and  $\mathcal{R}^{\epsilon}_{\mathrm{u,c}} = \epsilon \mathcal{R}^{\mathrm{s}}_{\mathrm{u,c}} + (1-\epsilon)\mathcal{R}^{\mathrm{c}}_{\mathrm{u,c}}$ . By exploiting the sandwich theorem, we can obtain the high-SNR slopes and diversity orders of any uplink SR-CR pair achieved through the time-sharing strategy, which are summarized in Table II. Denoting the achievable SR-CR pair as  $(\mathcal{R}_{\mathrm{s}},\mathcal{R}_{\mathrm{c}})$ , the uplink rate regions achieved by HISAC reads

$$\mathcal{C}_{\mathrm{u}} \!=\! \left\{\! \left(\mathcal{R}_{\mathrm{s}}, \mathcal{R}_{\mathrm{c}}\right) \,\middle|\, \mathcal{R}_{\mathrm{u,s}} \!\in\! \left[0, \mathcal{R}_{\mathrm{u,s}}^{\epsilon}\right], \mathcal{R}_{\mathrm{u,c}} \!\in\! \left[0, \mathcal{R}_{\mathrm{u,c}}^{\epsilon}\right], \epsilon \in\! \left[0, 1\right] \right\}. \tag{70}$$

## D. HMIMO based FDSAC

In uplink scenario, we also consider FDSAC as the baseline scheme, wherein  $\kappa \in [0,1]$  fraction of the total bandwidth is allocated to communications, and the other is used for sensing. Consequently, the SR achieved by FDSAC is given by  $\mathcal{R}_{\mathrm{u,s}}^{\mathrm{f}} = \frac{1-\kappa}{L}\log_2(1+\frac{1}{1-\kappa}p_\mathrm{s}/\sigma_\mathrm{u}^2L\alpha_\mathrm{s}\|\mathbf{h}_\mathrm{s}\|^4).$  As for communications, the CRs in the cases of I-CSI and S-CSI can be written as  $\mathcal{R}_{\mathrm{u,c}}^{\mathrm{f}} = \kappa\log_2(1+\frac{1}{\kappa}p_\mathrm{c}/\sigma_\mathrm{u}^2\|\mathbf{h}_\mathrm{c}\|^2)$  and  $\mathcal{R}_{\mathrm{u,c}}^{\mathrm{f}} = \kappa\log_2(1+\frac{1}{\kappa}p_\mathrm{c}/\sigma_\mathrm{u}^2\|\mathbf{v}_\star^{\mathbf{h}}\mathbf{h}_\mathrm{c}\|^2)$ , respectively. Note that the CR and SR achieved by FDSAC can be analyzed in a similar way we analyze those achieved by HISAC. For the sake of

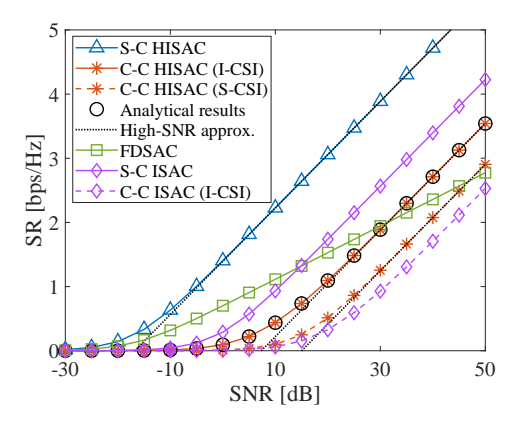


Fig. 3: Downlink SR.

reference, we summarize the results related to diversity order and high-SNR slope in Table II.

**Remark 19.** The results in Table II indicate that HISAC can achieve higher high-SNR slopes for both uplink SR and CR than FDSAC, providing more DoFs in terms of both S&C.

Finally, the SR-CR region of uplink FDSAC satisfies

$$\mathcal{C}_{\mathrm{u}}^{\mathrm{f}} = \left\{ (\mathcal{R}_{\mathrm{s}}, \mathcal{R}_{\mathrm{c}}) \, \middle| \mathcal{R}_{\mathrm{s}} \in [0, \mathcal{R}_{\mathrm{u,s}}^{\mathrm{f}}], \mathcal{R}_{\mathrm{c}} \in [0, \mathcal{R}_{\mathrm{u,c}}^{\mathrm{f}}], \kappa \in [0, 1] \right\}. \tag{71}$$

#### V. NUMERICAL RESULTS

In this section, numerical results are provided to evaluate the S&C performance of the proposed systems and verify the derived analytical results. Without otherwise specification, the simulation parameter settings are defined as follows:  $p/\sigma_{\rm s}^2=p/\sigma_{\rm c}^2=30$  dB,  $p_{\rm c}/\sigma_{\rm u}^2=p_{\rm s}/\sigma_{\rm u}^2=30$  dB,  $\alpha_0=0$  dB,  $\mathcal{R}_0=12$  bps/Hz,  $\lambda=0.125$  m,  $L_x=L_y=5\lambda,$   $d=\frac{\lambda}{4},$  L=4, and  $\kappa=\iota=0.5.$  The CU and the target are located at  $\mathbf{r}_{\rm c}=[1~{\rm m},1~{\rm m},5~{\rm m}]$  and  $\mathbf{r}_{\rm s}=[0~{\rm m},0~{\rm m},3~{\rm m}],$  respectively. For comparison, we also presents the simulation results for conventional MIMO based ISAC, referred to as "ISAC" in the plots, where the antenna spacing is set as  $d=\frac{5}{8}\lambda$  and the communication channels for each antenna are assumed as i.i.d. Rayleigh channels.

#### A. Downlink Performance

Fig. 2(a) and Fig. 2(b) plot the downlink CR and OP versus the communication SNR  $p/\sigma_c^2$ , respectively. It can be seen

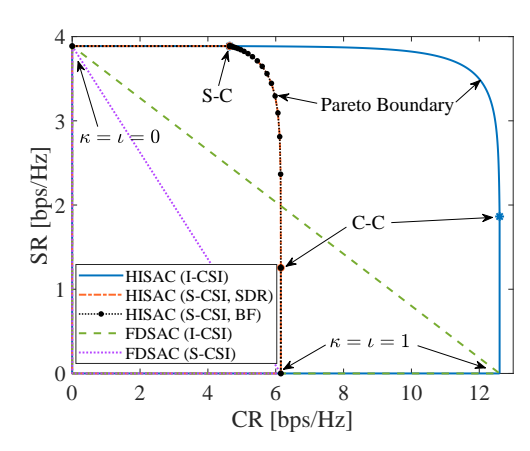


Fig. 4: Downlink rate regions.

that the C-C HISAC with I-CSI attains the best CR and OP, whereas FDSAC achieves the poorest communication performance. The derived analytical results match the simulation results well, and the high-SNR approximations precisely follow the simulation results in the high-SNR regime. Moreover, it is worth noting that regardless of the CSI assumption, the CRs of both C-C HISAC and S-C HISAC exhibit the same high-SNR slope, which is higher than that of FDSAC. However, under the I-CSI case, the downlink diversity order achieved by the C-C HISAC is significantly higher than the S-C HISAC, while the diversity orders achieved by different designs with S-CSI are identical. These observations validate the conclusions drawn in **Remark 7** and **11**.

Fig. 3 shows the downlink SR versus the sensing SNR  $p/\sigma_s^2$ , validating the accuracy of the analytical and approximated results. It is evident that S-C HISAC exhibits the most superior SR performance, while the SRs achieved by the S-C HISAC and the C-C HISAC yield the same high-SNR slope in both CSI cases. Through a joint examination of Fig. 2(a) and Fig. 3, we observe that both the CRs and SRs of HISAC demonstrate higher high-SNR slopes than FDSAC, aligning with the statement in **Remark 12**. Additionally, while the CSI has no impact on HISAC performance under the S-C design, it does influence the HISAC performance under the C-C design. Specifically, both CR and SR of the C-C design in the I-CSI case are larger than those in the S-CSI case, with the compensation of higher signaling overhead. It is also noticeable that the performance of downlink HISAC surpass conventional ISAC in terms of both S&C capabilities. In particular, with I-CSI, HISAC achieves higher CR and SR than ISAC, while both systems exhibit identical high-SNR slopes. On the other hand, for outage performance, due to the larger antenna spacing within the conventional MIMO resulting in fewer antennas ( $M = L_x/d \times L_y/d = 64$ ), the downlink diversity order of ISAC, which equals to the number of antennas [13], is lower than that of HISAC equivalent to the rank of  $\mathbf{R}$  (n = 88 under this setting).

In Fig. 4, the downlink SR-CR regions achieved by the HISAC system and the baseline FDSAC system with different CSI are presented. For HISAC with either I-CSI or S-CSI, the two marked points on the graph represent the S-C and C-C designs, respectively. The curve section connecting the two

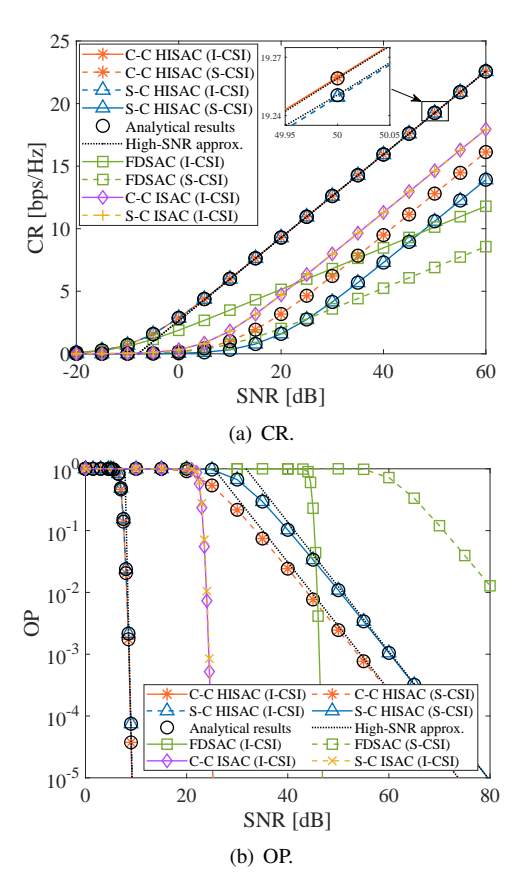


Fig. 5: Uplink communication performance.

points illustrates the Pareto boundary of the downlink HISAC's rate region, determined by solving either the problem (38) or (51) for values of  $\tau$  ranging from 0 to 1. As anticipated, it is evident that with I-CSI, HISAC can achieve a more extensive rate region than in the S-CSI case. Additionally, it is crucial to emphasize that in both CSI scenarios, the donwlink SR-CR region achieved by FDSAC is entirely encompassed by the rate region of HISAC. This observation highlights the superior S&C performance of HISAC compared to FDSAC. Last but not east, it can be seen from the above graph that for the S-CSI case, the rate region achieved by the SDR-based method is nearly coincident with that achieved by the bruteforce (BF) search-based Pareto optimal design. This means that the rank-one relaxation in problem (52) is tight in our considered system.

# B. Uplink Performance

Turning our attention to the uplink outcomes, we examine Fig 5(a) and Fig 5(b), which depict the uplink CR and OP with respect to the SNR  $p_{\rm c}/\sigma_{\rm u}^2$ , respectively. The analytical results closely match the simulation results, and the high-SNR approximations accurately capture the behavior in the high-SNR region. Notably, despite C-C HISAC with I-CSI exhibits the highest CR, the performance gap between uplink C-C HISAC and S-C HISAC under the I-CSI case is remarkably small when the correlation between the communication and sensing channels is minimal. Further, we observe that the CR of HISAC yields an identical high-SNR slope with both I-

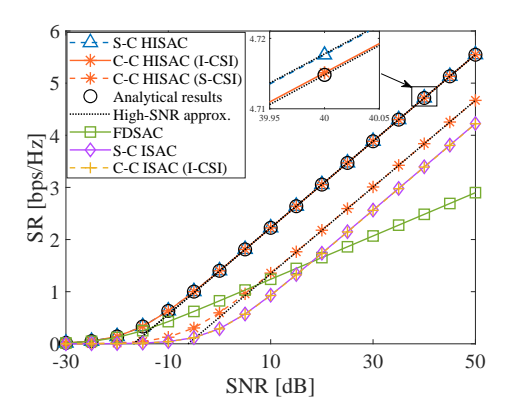


Fig. 6: Uplink SR.

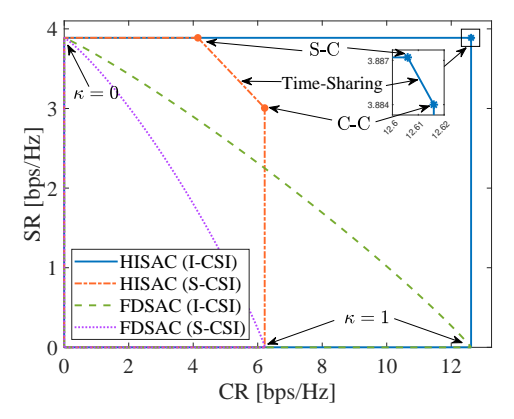


Fig. 7: Uplink rate regions.

CSI and S-CSI, which surpasses that achieved by FDSAC. On the other hand, the diversity orders achieved by HISAC with I-CSI are higher then those achieved under the S-CSI case, validating the discussions presented in Remark 15 and 18. Moreover, the diversity orders achieved by both HISAC and FDSAC are identical within the same CSI case, but the OPs of FDSAC are significantly lower than those of HISAC. In Fig. 6, we present the uplink SR as function of  $p_s/\sigma_u^2$ , which verifies the analytical and approximated results. It is worth noting that regardless of the SIC order, HISAC is capable of achieving higher high-SNR slopes than FDSAC, which is consistent with the statements in **Remark 19**. Importantly, compare to the conventional MIMO based ISAC, HISAC exhibits enhanced performance in S&C for uplink scenario. This underscores the advantages that HMIMO brings to ISAC systems.

Moving to Fig 7, we present the SR-CR regions attained by the uplink HISAC and FDSAC systems with both I-CSI and S-CSI. For the region of HISAC under either I-CSI or S-CSI case, the two points on the plot correspond to the rate pairs achieved by the S-C and C-C designs, respectively, while the line segment connecting these points represents the rates attainable through the time-sharing strategy between the two designs. A pivotal observation from the plot is that the rate region of uplink FDSAC is entirely encompassed within the rate region of uplink HISAC. This unequivocally demonstrates the superior performance of HISAC over FDSAC in the uplink scenario.

## VI. CONCLUSION

This paper has provided a comprehensive performance analysis of a HISAC system for both downlink and uplink scenarios. To account for the closed antenna spacing of the HMIMO, we considered the communication channels in a scattering environment as spatially correlated Rayleigh fading. Leveraging both I-CSI and S-CSI, we derived closed-form expressions and high-SNR approximations for the SRs, CRs, and OPs under the S-C and C-C designs. Furthermore, we identified the Pareto boundary of the downlink SR-CR region and characterized the uplink rate region using the time-sharing strategy. The high-SNR slopes and diversity orders of the proposed HISAC system and the baseline FDSAC system were obtained, providing further insights into system performance. The results have demonstrated that HISAC outperforms the conventional MIMO based ISAC and is able to achieve more DoFs and broader rate regions than the FDSAC in both downlink and uplink cases, underscoring the significant performance advantages offered by the HISAC system.

# APPENDIX

## A. Proof of Lemma 1

Vectorizing the echo signal  $\mathbf{Y}_{\mathrm{s}}$  yields

$$\text{vec}(\mathbf{Y}_{s}) = \sqrt{p} \mathbf{h}_{s}^{\mathsf{T}} \mathbf{w} \text{vec}(\mathbf{h}_{s} \mathbf{s}^{\mathsf{H}}) \beta + \text{vec}(\mathbf{N}_{s}).$$
 (A.1)

It is important to highlight that the conditional MI between  $\operatorname{vec}\left(\mathbf{Y}_{\mathrm{s}}\right)$  and  $\beta$  is equivalent to the capacity of a multipleinput single-output (MISO) Gaussian channel with a Gaussian distributed input  $\beta \sim \mathcal{CN}(0, \alpha_s)$ :  $\dot{\mathbf{y}} = \mathbf{h}\beta + \dot{\mathbf{n}}$ , where  $\dot{\mathbf{h}} = \sqrt{p} \mathbf{h}_{s}^{\mathsf{T}} \mathbf{w} \text{vec} (\mathbf{h}_{s} \mathbf{s}^{\mathsf{H}})$  denotes the channel vector, and  $\dot{\mathbf{n}} \sim \mathcal{CN}\left(\mathbf{0}, \sigma_{\mathrm{s}}^{2}\mathbf{I}\right)$ . Consequently, the sensing MI can be expressed as  $I(\mathbf{Y}_s; \beta | \mathbf{X}) = \log_2 \det(\mathbf{I} + \dot{\mathbf{h}}\dot{\mathbf{h}}^H/\sigma_s^2)$ . With the aid of Sylvester's identity, we have

$$I(\mathbf{Y}_{s}; \beta | \mathbf{X}) = \log_{2}(1 + \dot{\mathbf{h}}^{\mathsf{H}} \dot{\mathbf{h}} / \sigma_{s}^{2})$$
(A.2)

$$= \log_2(1 + p/\sigma_s^2 L \alpha_s ||\mathbf{h}_s||^2 |\mathbf{h}_s^\mathsf{T} \mathbf{w}|^2). \quad (A.3)$$

Substituting (A.3) into (7), we obtain the results in Lemma 1.

## B. Proof of Theorems 2 and 3

Notably, the communication channel can be written as  $h_c =$  $\mathbf{R}^{\frac{1}{2}}\overline{\mathbf{h}}$  with  $\overline{\mathbf{h}} \sim \mathcal{CN}(\mathbf{0}, \mathbf{I}_N)$ . Since  $\mathbf{h}_s$  is irrelevant to  $\mathbf{h}_c$ , we have  $\mathbf{h}_{s}^{\mathsf{H}}\mathbf{h}_{c} = \mathbf{h}_{s}^{\mathsf{H}}\mathbf{R}^{\frac{1}{2}}\overline{\mathbf{h}} \sim \mathcal{CN}(0, \mathbf{h}_{s}^{\mathsf{H}}\mathbf{R}\mathbf{h}_{s})$ . Hence,  $|\mathbf{h}_{s}^{\mathsf{H}}\mathbf{h}_{c}|^{2}$  is exponentially distributed with its probability density function (PDF) given by  $\frac{1}{\mathbf{h}_{s}^{H}\mathbf{R}\mathbf{h}_{s}}e^{-\frac{x}{\mathbf{h}_{s}^{H}\mathbf{R}\mathbf{h}_{s}}}$ . Consequently, based on (22), the ECR can be calculated as follows:  $\mathcal{R}_{d,c}^{s} = \frac{1}{\mathbf{h}_{s}^{H}\mathbf{R}\mathbf{h}_{s}\ln 2} \int_{0}^{\infty} \ln \left(1 + p/\sigma_{c}^{2} \|\mathbf{h}_{s}\|^{-2} x\right) e^{-\frac{x}{\mathbf{h}_{s}^{H}\mathbf{R}\mathbf{h}_{s}}} dx.$ 

$$\mathcal{R}_{d,c}^{s} = \frac{1}{\mathbf{h}_{s}^{\mathsf{H}} \mathbf{R} \mathbf{h}_{s} \ln 2} \int_{0}^{\infty} \ln \left( 1 + p / \sigma_{c}^{2} \left\| \mathbf{h}_{s} \right\|^{-2} x \right) e^{-\frac{x}{\mathbf{h}_{s}^{\mathsf{H}} \mathbf{R} \mathbf{h}_{s}}} dx.$$
(B.1)

With the aid of [22, (4.337.2)], the results in (23) can be derived. When  $p \to \infty$ , by applying the fact of  $\lim_{x\to\infty} \log_2(1+$  $(x) \approx \log_2 x$ , we have

$$\mathcal{R}_{\mathrm{d,c}}^{\mathrm{s}} \approx \frac{1}{\mathbf{h}_{\mathrm{s}}^{\mathsf{H}} \mathbf{R} \mathbf{h}_{\mathrm{s}} \ln 2} \int_{0}^{\infty} \ln \left( p / \sigma_{\mathrm{c}}^{2} \left\| \mathbf{h}_{\mathrm{s}} \right\|^{-2} x \right) e^{-\frac{x}{\mathbf{h}_{\mathrm{s}}^{\mathsf{H}} \mathbf{R} \mathbf{h}_{\mathrm{s}}}} dx. \tag{B.2}$$

With the aid of [22, (4.331.1)], we can obtain (24).

By substituting (22) into (25), the OP can be obtained as

$$\mathcal{P}_{d}^{s} = F_{|\mathbf{h}_{s}^{\mathsf{H}}\mathbf{h}_{c}|^{2}} \left( \sigma_{c}^{2} \|\mathbf{h}_{s}\|^{2} \left( 2^{\mathcal{R}_{0}} - 1 \right) / p \right),$$
 (B.3)

where  $F_{|\mathbf{h}^{\mathsf{H}}\mathbf{h}_{\mathsf{o}}|^2}(x) = 1 - \mathrm{e}^{-\frac{x}{\mathbf{h}_{\mathsf{s}}^{\mathsf{H}}\mathbf{R}\mathbf{h}_{\mathsf{s}}}}$  represents the cumulative distribution function (CDF) of  $|\mathbf{h}_{s}^{\mathsf{H}}\mathbf{h}_{c}|^{2}$  following an exponential distribution. The high-SNR approximation can be easily obtained by applying  $\lim_{x\to 0} \exp(-x) = 1 - x$  [22, (1.211.1)].

# C. Proof of Theorems 4 and 5

Based on (13), by defining  $\overline{\mathbf{h}} \triangleq [h_1, \dots, h_n]^H$ , the communication channel gain  $\|\mathbf{h}_{c}\|^{2}$  can be expressed as follows:

$$\|\mathbf{h}_{c}\|^{2} = \overline{\mathbf{h}}^{\mathsf{H}} \mathbf{\Sigma} \overline{\mathbf{h}} = \sum_{n=1}^{\mathsf{n}} \lambda_{n} |h_{n}|^{2}. \tag{C.1}$$

Note that  $\{h_n\}_{n=1,\dots,n}$  contains n independent complex Gaussian variables with  $h_n \sim \mathcal{CN}(0,1)$ . Therefore, the PDF of  $\sum_{n=1}^{n} \lambda_n |h_n|^2$ , which is the sum of n independent exponentially distributed variables, is given by [23]

$$f_{\|\mathbf{h}_{c}\|^{2}}(x) = \frac{\lambda_{n}^{n}}{\prod_{n=1}^{n} \lambda_{n}} \sum_{k=0}^{\infty} \frac{\delta_{k} x^{n+k-1}}{\lambda_{n}^{n+k} (n+k)!} e^{-\frac{x}{\lambda_{n}}}.$$
 (C.2)

With the aid of [22, (3.351.1)], we can calculated the CDF of  $\|\mathbf{h}_{\mathrm{c}}\|^2$  as

$$F_{\parallel \mathbf{h}_c \parallel^2}(x) = \frac{\lambda_{\mathsf{n}}^{\mathsf{n}}}{\prod_{n=1}^{\mathsf{n}} \lambda_n} \sum_{k=0}^{\infty} \frac{\delta_k \Upsilon(\mathsf{n} + k, \frac{x}{\lambda_n})}{(\mathsf{n} + k - 1)!}.$$
 (C.3)

Subsequently, the OP is given by

$$\mathcal{P}_{d}^{c} = \Pr\left(\|\mathbf{h}_{c}\|^{2} < \frac{2^{\mathcal{R}_{0}} - 1}{p/\sigma_{c}^{2}}\right) = F_{\|\mathbf{h}_{c}\|^{2}}\left(\frac{2^{\mathcal{R}_{0}} - 1}{p/\sigma_{c}^{2}}\right).$$
 (C.4)

When  $p \to \infty$ , by utilizing the asymptotic property of the lower incomplete gamma function [22, (8.354.1)], i.e.,  $\lim_{x\to\infty} \Upsilon(s,x) \simeq \frac{x^s}{s}$ , within (30), we can obtain (31). Moreover, the ECR can be calculated as

$$\mathcal{R}_{d,c}^{c} = \int_{0}^{\infty} \log_{2} \left( 1 + p / \sigma_{c}^{2} x \right) f_{\|\mathbf{h}_{c}\|^{2}} (x) dx.$$
 (C.5)

With the aid of [22, (4.337.5)], we can obtain (33). When  $p \to \infty$ , by leveraging  $\lim_{x \to \infty} \log_2(1+x) \simeq \log_2 x$  and [22, (4.352.1)], the high-SNR approximation can be derived.

## D. Proof of Theorem 6

By performing some manipulations based on (35), the average SR can be written as

$$\mathcal{R}_{d,s}^{c} = \mathbb{E}\{\overline{\mathcal{R}}_{d,s}^{c}\} = \frac{1}{L} \left( \underbrace{\mathbb{E}\{\log_{2}(\overline{\mathbf{h}}^{\mathsf{H}} \Delta \overline{\mathbf{h}})\}}_{P_{1}} - \underbrace{\mathbb{E}\{\log_{2}(\|\mathbf{h}_{c}\|^{2})\}}_{P_{2}} \right), \tag{D.1}$$

Upon applying ED to  $\Delta$ , i.e.,  $\Delta = \mathbf{Q}\Lambda\mathbf{Q}^{\mathsf{H}}$ , where  $\mathbf{Q}$ is unitary and  $\Lambda = \text{diag}\{\lambda_{\Delta,1},\ldots,\lambda_{\Delta,t},0,\ldots,0\}$  with  $t = rank(\Delta)$ , and defining  $Q^H \overline{h} \triangleq [z_1, \dots, z_N]^H$ , where  $\{z_n\}_{n=1,\dots,N}$  contains N independent complex Gaussian variables with  $z_n \sim \mathcal{CN}(0,1)$ , we can rewrite  $P_1$  as follows:

$$P_{1} = \mathbb{E}\{\log_{2}(\overline{\mathbf{h}}^{\mathsf{H}}\mathbf{Q}\boldsymbol{\Lambda}\mathbf{Q}^{\mathsf{H}}\overline{\mathbf{h}})\} = \mathbb{E}\left\{\log_{2}\left(\sum_{t=1}^{\mathsf{t}}\lambda_{\Delta,t}\left|z_{t}\right|^{2}\right)\right\}.$$

Consequently, both (D.2) and  $P_2$  can be calculated by following the similar steps in Appendix C. When  $p \to \infty$ , the results of (37) can be obtained by following the similar steps of the high-SNR approximation derivation in Appendix B.

#### E. Proof of Theorem 7

Based on the Karush-Kuhn-Tucker conditions, we have

$$\begin{cases} \nabla(-\mathcal{R}) + \lambda \nabla(\|\mathbf{w}\|^2 - 1) + \mu_1 \nabla f_1 + \mu_2 \nabla f_2 = \mathbf{0}, & (E.1) \end{cases}$$

$$\mu_1 f_1 = 0, \ \mu_2 f_2 = 0, \ \mu_1 \geqslant 0, \ \mu_2 \geqslant 0,$$
 (E.2)

where  $f_1 = 2^{(1-\tau)\mathcal{R}} - 1 - |\mathbf{h}_1^\mathsf{T} \mathbf{w}|^2$ ,  $f_2 = 2^{\tau L \mathcal{R}} - 1 - |\mathbf{h}_2^\mathsf{T} \mathbf{w}|^2$ , and  $\lambda$ ,  $\mu_1$ ,  $\mu_2$  are real Lagrangian multipliers. Based on (E.1),

$$\mu_1 \mathbf{h}_1^* \mathbf{h}_1^{\mathsf{I}} \mathbf{w} + \mu_2 \mathbf{h}_2^* \mathbf{h}_2^{\mathsf{I}} \mathbf{w} = \lambda \mathbf{w}, \tag{E.3}$$

$$\begin{cases} \mu_1 \mathbf{h}_1^* \mathbf{h}_1^\mathsf{T} \mathbf{w} + \mu_2 \mathbf{h}_2^* \mathbf{h}_2^\mathsf{T} \mathbf{w} = \lambda \mathbf{w}, & (E.3) \\ \mu_1 |\mathbf{h}_1^\mathsf{T} \mathbf{w}|^2 + \mu_2 |\mathbf{h}_2^\mathsf{T} \mathbf{w}|^2 = \lambda \mathbf{w}^\mathsf{H} \mathbf{w} = \lambda, & (E.4) \\ \mu_1 2^{(1-\tau)\mathcal{R}} (1-\tau) \ln 2 + \mu_2 2^{\tau L \mathcal{R}} \tau L \ln 2 = 1. & (E.5) \end{cases}$$

$$\mu_1 2^{(1-\tau)\mathcal{R}} (1-\tau) \ln 2 + \mu_2 2^{\tau L \mathcal{R}} \tau L \ln 2 = 1. \quad (E.5)$$

It can be concluded from (E.5) that  $\mu_1$  and  $\mu_2$  cannot be 0 at the same time. Therefore, we discuss three cases as follows.

Case 1:  $\mu_1 > 0$  and  $\mu_2 = 0$ : In this case, we have

$$(E.6)$$

$$\mu_1 |\mathbf{h}_1^\mathsf{T} \mathbf{w}|^2 = \lambda, \tag{E.7}$$

$$\begin{cases} \mu_{1} | \mathbf{h}_{1}^{\mathsf{T}} \mathbf{w} |^{2} = \lambda, & \text{(E.8)} \\ \mu_{1} | \mathbf{h}_{1}^{\mathsf{T}} \mathbf{w} |^{2} = \lambda, & \text{(E.7)} \\ \mu_{1} 2^{(1-\tau)\mathcal{R}} (1-\tau) \ln 2 = 1, & \text{(E.8)} \\ f_{2} = 0 \Rightarrow |\mathbf{w}^{\mathsf{H}} \mathbf{h}_{1}|^{2} = 2^{(1-\tau)\mathcal{R}} - 1. & \text{(E.9)} \end{cases}$$

$$f_2 = 0 \Rightarrow |\mathbf{w}^{\mathsf{H}} \mathbf{h}_1|^2 = 2^{(1-\tau)\mathcal{R}} - 1.$$
 (E.9)

Based on the above conditions, the optimal value of w and  $\mathcal{R}$  are given by  $\mathbf{w}_{\tau} = \|\mathbf{h}_{c}\|^{-1}\mathbf{h}_{c}^{*}$  and  $\mathcal{R}^{*} = \frac{1}{1-\tau}\log(1+\tau)$  $\|\mathbf{h}_1\|^2) = \overline{\mathcal{R}}_{d,c}^c/(1-\tau)$ , respectively. Accordingly, the SR sat-

isfies  $\overline{\mathcal{R}}_{d,s}^c \geqslant \tau \mathcal{R}^\star$ , which yields  $\tau \in [0, \overline{\mathcal{R}}_{d,s}^c / (\overline{\mathcal{R}}_{d,c}^c + \overline{\mathcal{R}}_{d,s}^c)]$ . Case 2:  $\mu_1 = 0$  and  $\mu_2 > 0$ : Similar to Case 1, we can obtain  $\mathcal{R}^\star = \frac{\mathcal{R}_{d,s}^s}{\tau}$  and  $\mathbf{w}_\tau = \|\mathbf{h}_s\|^{-1}\mathbf{h}_s^\star$  for  $\tau \in [\mathcal{R}_{d,s}^s / (\overline{\mathcal{R}}_{d,c}^s + \overline{\mathcal{R}}_{d,s}^s)]$ 

Case 3:  $\mu_1 > 0$  and  $\mu_2 > 0$ : In this case, we have  $f_1 = 0 \Rightarrow |\mathbf{h}_1^\mathsf{T} \mathbf{w}|^2 = 2^{(1-\tau)\mathcal{R}} - 1$  and  $f_2 = 0 \Rightarrow |\mathbf{h}_2^\mathsf{T} \mathbf{w}|^2 = 2^{\tau L \mathcal{R}} - 1$ . From (E.3), we have  $\mathbf{w} = \frac{\mu_1 \mathbf{h}_1^\mathsf{T} \mathbf{w}}{\lambda} \mathbf{h}_1^* + \frac{\mu_2 \mathbf{h}_2^\mathsf{T} \mathbf{w}}{\lambda} \mathbf{h}_2^* \triangleq a \mathbf{h}_1^* + 1$  $b\mathbf{h}_{2}^{*}$ , which further yields

$$\mu_1(\|\mathbf{h}_1\|^2 + b/a\rho) = \mu_2(\|\mathbf{h}_2\|^2 + a/b\rho^*) = \lambda,$$
 (E.10)

where  $\frac{a}{b} = \frac{\mu_1 \sqrt{2^{(1-\tau)\mathcal{R}} - 1}}{\mu_2 \sqrt{2^{\tau L \mathcal{R}} - 1} e^{-j \angle \rho}}$ . By combining (E.10) and (E.5), we can derive  $\mu_1 = \frac{\xi_2}{\chi}$ ,  $\mu_2 = \frac{\xi_1}{\chi}$ , and  $\lambda = \frac{\|\mathbf{h}_1\|^2 \|\mathbf{h}_2\|^2 - \rho^2}{\chi}$ . Additionally, upon substituting the above results of  $\mu_1$ ,  $\mu_2$ 

and  $\lambda$  into (E.4), we obtain an equation for  $\mathcal{R}$  as follows:

$$\xi_1(2^{\tau L \mathcal{R}} - 1) + \xi_2(2^{(1-\tau)\mathcal{R}} - 1) = \|\mathbf{h}_1\|^2 \|\mathbf{h}_2\|^2 - |\rho|^2.$$
(F.11)

Since  $\xi_1(2^{\tau LR}-1)+\xi_2(2^{(1-\tau)R}-1)$  is a monotonic function with respect to  $\mathcal{R}$ , ranging from 0 to  $\infty$ , the optimal solution  $\mathcal{R} = \mathcal{R}^{\star}$  can be obtained by solving (E.11), and  $w_{\tau}$  follows immediately.

#### F. Proof of Lemma 2

As BS dose not know h<sub>c</sub>, the C-C design of w is irrelevant to  $\mathbf{h}_{c}$ , which yields  $\mathbf{w}^{\mathsf{H}}\mathbf{h}_{c} = \mathbf{w}^{\mathsf{H}}\mathbf{R}^{\frac{1}{2}}\overline{\mathbf{h}} \sim \mathcal{CN}(0, \mathbf{w}^{\mathsf{H}}\mathbf{R}\mathbf{w}).$ Hence,  $|\mathbf{w}^{\mathsf{H}}\mathbf{h}_{\mathrm{c}}|^2$  is exponentially distributed with its PDF given by  $\frac{1}{\mathbf{w}^H \mathbf{R} \mathbf{w}} e^{-\frac{x}{\mathbf{w}^H \mathbf{R} \mathbf{w}}}$ . Consequently, the ECR in (42) can

$$\mathbb{E}\{\overline{\mathcal{R}}_{d,c}\} = \int_0^\infty \log_2(1 + p/\sigma_c^2 x) \frac{1}{\mathbf{w}^{\mathsf{H}} \mathbf{R} \mathbf{w}} e^{-\frac{x}{\mathbf{w}^{\mathsf{H}} \mathbf{R} \mathbf{w}}} dx \quad (G.1)$$
$$= \int_0^\infty \log_2(1 + p/\sigma_c^2 \mathbf{w}^{\mathsf{H}} \mathbf{R} \mathbf{w} x) e^{-x} dx, \quad (G.2)$$

which is monotone increasing with  $\mathbf{w}^{\mathsf{H}}\mathbf{R}\mathbf{w}$ . Consequently, the problem in (42) is equivalent to

$$\mathbf{w} = \operatorname{argmax}_{\|\mathbf{w}\|^2 = 1} \mathbf{w}^{\mathsf{H}} \mathbf{R} \mathbf{w} = \mathbf{u}, \tag{G.3}$$

where  $\mathbf{u} \in \mathbb{C}^{N \times 1}$  is used to denote the principal eigenvector of  $\mathbf{R}$ . Furthermore, based on the ED of  $\mathbf{R}$  shown in (14), it is trivial that  $\mathbf{u} = \mathbf{a}_{\star}$ .

#### G. Proof of Lemma 3

The superposed uplink S&C signal reads  $\mathbf{Y} = \sqrt{p_s}\beta\mathbf{h}_s\mathbf{h}_s^\mathsf{T}\mathbf{w}\mathbf{s}_s^\mathsf{H} + \mathbf{Z}_c$ . Vectorizing this signal yields

$$\mathsf{vec}(\mathbf{Y}) = \sqrt{p_{\mathrm{s}}} \mathbf{h}_{\mathrm{s}}^{\mathsf{T}} \mathbf{w} \mathbf{h}_{\mathrm{v}} \beta + \mathbf{z}_{\mathrm{c}}, \tag{H.1}$$

where  $\mathbf{h}_{\rm v} = \text{vec}(\mathbf{h}_{\rm s}\mathbf{s}_{\rm s}^{\sf H})$  and  $\mathbf{z}_{\rm c} = \text{vec}(\mathbf{Z}_{\rm c})$ . By treating (H.1) as a MISO channel model with Gaussian noise  $\mathbf{z}_{\rm c}$ , the SR can be written as follows:

$$\overline{\mathcal{R}}_{\mathrm{u.s}}^{\mathrm{c}} = L^{-1} \log_2(1 + \alpha_{\mathrm{s}} p_{\mathrm{s}} |\mathbf{h}_{\mathrm{s}}^{\mathsf{T}} \mathbf{w}|^2 \mathbf{h}_{\mathrm{v}}^{\mathsf{H}} \mathbb{E}^{-1} \{ \mathbf{z}_{\mathrm{c}} \mathbf{z}_{\mathrm{c}}^{\mathsf{H}} \} \mathbf{h}_{\mathrm{v}} ). \quad (\mathrm{H.2})$$

Recall that  $\mathbf{Z}_c = \sqrt{p_c}\mathbf{h}_c\mathbf{s}_c^\mathsf{H} + \mathbf{N}_u$ , which together with the fact that  $\mathbb{E}\{\mathbf{s}_c\mathbf{s}_c^\mathsf{H}\} = \mathbf{I}$ , yields  $\mathbb{E}\{\mathbf{z}_c\mathbf{z}_c^\mathsf{H}\} = \mathbf{I} \otimes (p_c\mathbf{h}_c\mathbf{h}_c^\mathsf{H} + \sigma_u^2\mathbf{I})$ . By further exploiting the fact that  $L^{-1}\|\mathbf{s}_s\|^2 = 1$ , we obtain

$$\mathbf{h}_{v}^{\mathsf{H}} \mathbb{E}^{-1} \{ \mathbf{z}_{c} \mathbf{z}_{c}^{\mathsf{H}} \} \mathbf{h}_{v} = \mathbf{h}_{s}^{\mathsf{H}} (p_{c} \mathbf{h}_{c} \mathbf{h}_{c}^{\mathsf{H}} + \sigma_{u}^{2} \mathbf{I})^{-1} \mathbf{h}_{s} \| \mathbf{s}_{s} \|^{2}. \quad (H.3)$$

By harnessing the Woodbury matrix identity, we have  $(p_{\rm c}\mathbf{h}_{\rm c}\mathbf{h}_{\rm c}^{\sf H}+\sigma_{\rm u}^2\mathbf{I})^{-1}=\frac{1}{\sigma_{\rm u}^2}(\mathbf{I}-\frac{p_{\rm c}}{p_{\rm c}\|\mathbf{h}_{\rm c}\|^2+\sigma_{\rm u}^2}\mathbf{h}_{\rm c}\mathbf{h}_{\rm c}^{\sf H})$ . The final results follow immediately.

## H. Proof of Theorem 12

To achieve the optimal SR, we have  $\mathbf{w} = \mathbf{h}_s ||\mathbf{h}_s||^{-1}$ , and thus the received signal of the BS at the  $\ell$ th time slot reads

$$\mathbf{y}_{\ell} = \sqrt{p_{c}}\mathbf{h}_{c}\mathbf{s}_{c,\ell} + \underbrace{\sqrt{p_{s}}\beta\mathbf{h}_{s}\|\mathbf{h}_{s}\|\mathbf{s}_{s,\ell} + \mathbf{n}_{u,\ell}}_{\mathbf{z}_{s,\ell}}$$
(I.1)

for  $\ell=1,\ldots,L$ , where  $\mathbf{n}_{\mathrm{u},\ell}\sim\mathcal{CN}(\mathbf{0},\sigma_{\mathrm{u}}^2\mathbf{I})$  is the  $\ell$ th column of  $\mathbf{N}_{\mathrm{u}}$ . By treating  $\mathbf{z}_{\mathrm{s},\ell}$  as a zero-mean Gaussian random variable, we calculate the CR as follows:

$$\overline{\mathcal{R}}_{u,c}^{s} = \log_2(1 + p_c \mathbf{h}_c^{\mathsf{H}} \mathbb{E} \{ \mathbf{z}_{s,\ell} \mathbf{z}_{s,\ell}^{\mathsf{H}} \}^{-1} \mathbf{h}_c)$$
 (I.2)

with  $\mathbb{E}\{\mathbf{z}_{\mathrm{s},\ell}\mathbf{z}_{\mathrm{s},\ell}^{\mathsf{H}}\}=p_{\mathrm{s}}\alpha_{\mathrm{s}}\|\mathbf{h}_{\mathrm{s}}\|^{2}\mathbf{h}_{\mathrm{s}}\mathbf{h}_{\mathrm{s}}^{\mathsf{H}}+\sigma_{\mathrm{u}}^{2}\mathbf{I}$ , which is independent with the time slot. Hence, the ECR is given by  $\mathcal{R}_{\mathrm{u,c}}^{\mathrm{s}}=\mathbb{E}\{\overline{\mathcal{R}}_{\mathrm{u,c}}^{\mathrm{s}}\}$ , which can be analyzed by following the similar steps presented in Appendix C.

#### I. Proof of Lemma 4

As  $\mathbf{h}_c$  is unknown to the BS, the design of  $\mathbf{v}$  is irrelevant to  $\mathbf{h}_c$ , which yields  $\mathbf{v}^H\mathbf{h}_c = \mathbf{v}^H\mathbf{R}^{\frac{1}{2}}\overline{\mathbf{h}} \sim \mathcal{CN}(0,\mathbf{v}^H\mathbf{R}\mathbf{v})$ . Hence,  $\frac{p_c|\mathbf{v}^H\mathbf{h}_c|^2}{p_s\alpha_s\|\mathbf{h}_s\|^2|\mathbf{v}^H\mathbf{h}_s|^2+\sigma_u^2}$  is exponentially distributed. Based on the property of exponential distribution, maximizing the ECR  $\mathbb{E}\{\overline{\mathcal{R}}_{u,c}^S\}$  is equivalent to maximizing the expectation of  $\frac{p_c|\mathbf{v}^H\mathbf{h}_c|^2}{p_s\alpha_s\|\mathbf{h}_s\|^2|\mathbf{v}^H\mathbf{h}_s|^2+\sigma_u^2}$ , which yields

$$\mathbf{v}_{\star} = \operatorname{argmax}_{\|\mathbf{v}\|^{2}=1} \mathbb{E} \left\{ \frac{p_{c} |\mathbf{v}^{\mathsf{H}} \mathbf{h}_{c}|^{2}}{p_{s} \alpha_{s} \|\mathbf{h}_{s}\|^{2} |\mathbf{v}^{\mathsf{H}} \mathbf{h}_{s}|^{2} + \sigma_{u}^{2}} \right\}$$

$$= \operatorname{argmax}_{\|\mathbf{v}\|^{2}=1} \frac{\mathbf{v}^{\mathsf{H}} \mathbf{R} \mathbf{v}}{\mathbf{v}^{\mathsf{H}} (p_{s} / \sigma_{u}^{2} \alpha_{s} \|\mathbf{h}_{s}\|^{2} \mathbf{h}_{s} \mathbf{h}_{s}^{\mathsf{H}} + \mathbf{I}) \mathbf{v}}. \quad (J.1)$$

By applying the Rayleigh quotient theorem, we can obtain the expression of  $\mathbf{v}_{\star}$ . Besides, it can be concluded that  $\frac{\mathbf{v}_{\star}^{\mathsf{H}}\mathbf{v}_{\star}}{\mathbf{v}_{\star}^{\mathsf{H}}(p_{\mathrm{s}}/\sigma_{\mathrm{u}}^{2}\alpha_{\mathrm{s}}\|\mathbf{h}_{\mathrm{s}}\|^{2}\mathbf{h}_{\mathrm{s}}\mathbf{h}_{\mathrm{s}}^{\mathsf{H}}+\mathbf{I})\mathbf{v}_{\star}}=\varkappa$ , where  $\varkappa$  denotes the principal eigenvalue of  $(p_{\mathrm{s}}/\sigma_{\mathrm{u}}^{2}\alpha_{\mathrm{s}}\|\mathbf{h}_{\mathrm{s}}\|^{2}\mathbf{h}_{\mathrm{s}}\mathbf{h}_{\mathrm{s}}^{\mathsf{H}}+\mathbf{I})^{-\frac{1}{2}}\mathbf{R}(p_{\mathrm{s}}/\sigma_{\mathrm{u}}^{2}\alpha_{\mathrm{s}}\|\mathbf{h}_{\mathrm{s}}\|^{2}\mathbf{h}_{\mathrm{s}}\mathbf{h}_{\mathrm{s}}^{\mathsf{H}}+\mathbf{I})^{-\frac{1}{2}}$ .

#### REFERENCES

- J. A. Zhang et al., "An overview of signal processing techniques for joint communication and radar sensing," *IEEE J. Sel. Topics Signal Process.*, vol. 15, no. 6, pp. 1295–1315, Nov. 2021.
- [2] A. Liu et al., "A survey on fundamental limits of integrated sensing and communication," *IEEE Commun. Surveys Tuts.*, vol. 24, no. 2, pp. 994–1034, Feb. 2022.
- [3] Z. Wei et al., "Integrated sensing and communication signals toward 5G-A and 6G: A survey," *IEEE Internet Things J.*, vol. 10, no. 13, pp. 11068–11092, Jul. 2023.
- [4] C. Huang et al., "Holographic MIMO surfaces for 6g wireless networks: Opportunities, challenges, and trends," *IEEE Wireless Commun.*, vol. 27, no. 5, pp. 118–125, Oct. 2020.
- [5] O. T. Demir et al., "Channel modeling and channel estimation for holographic massive MIMO with planar arrays," *IEEE Wireless Commun. Lett.*, vol. 11, no. 5, pp. 997–1001, May 2022.
- [6] A. Pizzo, T. L. Marzetta, and L. Sanguinetti, "Spatially-stationary model for holographic MIMO small-scale fading," *IEEE J. Sel. Areas Commun.*, vol. 38, no. 9, pp. 1964–1979, Sep. 2020.
- [7] H. Zhang et al., "Holographic integrated sensing and communications: Principles, technology, and implementation," *IEEE Commun. Mag.*, vol. 61, no. 5, pp. 83–89, May 2023.
- [8] —, "Holographic integrated sensing and communication," *IEEE J. Sel. Areas Commun.*, vol. 40, no. 7, pp. 2114–2130, Jul. 2022.
- [9] J. Hu, Z. Chen, and J. Luo, "Multi-band reconfigurable holographic surface based ISAC systems: Design and optimization," in *Proc. IEEE Int. Conf. Commun. (ICC)*, 2023, pp. 2927–2932.
- [10] C. Ouyang, Y. Liu, H. Yang, and N. Al-Dhahir, "Integrated sensing and communications: A mutual information-based framework," *IEEE Commun. Mag.*, vol. 61, no. 5, pp. 26–32, May 2023.
- [11] A. R. Chiriyath, B. Paul, G. M. Jacyna, and D. W. Bliss, "Inner bounds on performance of radar and communications co-existence," *IEEE Trans. Signal Process.*, vol. 64, no. 2, pp. 464–474, Jan. 2016.
- [12] M. Liu *et al.*, "Performance analysis and power allocation for cooperative ISAC networks," *IEEE Internet Things J.*, vol. 10, no. 7, pp. 6336–6351, Apr. 2023.
- [13] C. Ouyang et al., "Revealing the impact of beamforming in ISAC," IEEE Wireless Commun. Lett., vol. 13, no. 2, pp. 362–366, Feb. 2024.
- [14] ——, "On the performance of uplink ISAC systems," *IEEE Commun. Lett.*, vol. 26, no. 8, pp. 1769–1773, Aug. 2022.
- [15] A. Pizzo, L. Sanguinetti, and T. L. Marzetta, "Fourier plane-wave series expansion for holographic MIMO communications," *IEEE Trans. Wireless Commun.*, vol. 21, no. 9, pp. 6890–6905, Sep. 2022.
- [16] D. Starer and A. Nehorai, "Passive localization of near-field sources by path following," *IEEE Trans. Signal Process.*, vol. 42, no. 3, pp. 677–680, Mar. 1994.
- [17] B. Tang and J. Li, "Spectrally constrained MIMO radar waveform design based on mutual information," *IEEE Trans. Signal Process.*, vol. 67, no. 3, pp. 821–834, Feb. 2019.
- [18] R. Zhang and S. Cui, "Cooperative interference management with MISO beamforming," *IEEE Trans. Signal Process.*, vol. 58, no. 10, pp. 5450– 5458, Oct. 2010.
- [19] Z.-Q. Luo et al., "Semidefinite relaxation of quadratic optimization problems," *IEEE Signal Process. Mag.*, vol. 27, no. 3, pp. 20–34, May 2010.
- [20] B. Hassibi and B. Hochwald, "How much training is needed in multipleantenna wireless links?" *IEEE Trans. Inf. Theory*, vol. 49, no. 4, pp. 951–963, Apr 2003.
- [21] R. W. Heath Jr and A. Lozano, Foundations of MIMO communication. Cambridge, U.K.: Cambridge Univ. Press, 2018.
- [22] I. S. Gradshteyn and I. M. Ryzhik, Table of Integrals, Series and Products, 7th ed. New York, NY, USA: Academic Press, 2007.
- [23] P. G. Moschopoulos, "The distribution of the sum of independent gamma random variables," Ann. Inst. Statist. Math., vol. 37, no. 1, pp. 541–544, 1985